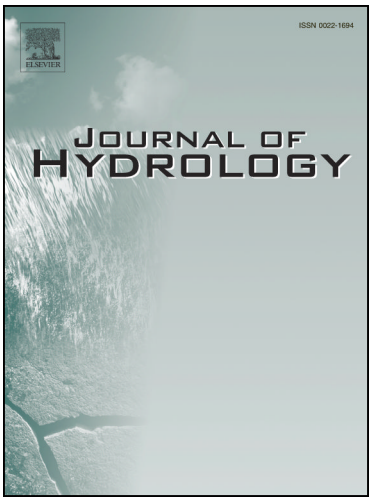

Research papers

Groundwater dynamics at the hillslope – riparian interface in a year with extreme winter rainfall

B. Scheliga, D. Tetzlaff, G. Nuetzmann, C. Soulsby

PII: S0022-1694(18)30504-3
DOI: https://doi.org/10.1016/j.jhydrol.2018.06.082
Reference: HYDROL 22931

To appear in: *Journal of Hydrology*

Received Date: 13 February 2018
Revised Date: 31 May 2018
Accepted Date: 29 June 2018

Please cite this article as: Scheliga, B., Tetzlaff, D., Nuetzmann, G., Soulsby, C., Groundwater dynamics at the hillslope – riparian interface in a year with extreme winter rainfall, *Journal of Hydrology* (2018), doi: https://doi.org/10.1016/j.jhydrol.2018.06.082

Groundwater dynamics at the hillslope – riparian interface in a year with extreme winter rainfall

B. Scheliga[1], D. Tetzlaff [1,2,3], G. Nuetzmann[2] and C. Soulsby [1,2]

[1] Northern Rivers Institute, School of Geosciences, University of Aberdeen, AB24 3UF, UK.

[2] Leibniz Institute of Freshwater Ecology and Inland Fisheries, Berlin, 12587, Germany.

[3] Department of Geography, Humboldt University Berlin, Berlin, 10099, Germany.

Abstract

Water movement in hillslopes is determined by the subsurface characteristics that control flow paths connecting precipitation to stream flow generation. The hydrological response of hillslopes is notoriously non-linear and non-stationary; with the relative importance of vertical and lateral flow paths also depending on event characteristics and antecedent conditions. In northern boreal regions, climate change projections indicate that wetter and warmer winter conditions are likely to generate more extreme flood events. Here, we report a study from an upland catchment in northern Scotland where a monitoring year provided an opportunity to contextualise observations during the hillslope response to a winter rainfall event that locally caused the most extreme flooding for over 200 years. Monitoring the hillslope water table, soil moisture and isotopes in precipitation, groundwater and stream flow provided invaluable insight into hillslope – riparian coupling. Groundwater with a shallow water table (<0.05 m deep) in poorly drained valley bottom drift deposits maintained almost fully saturated and stream-connected peat soil profiles in riparian areas. In the wettest periods, the groundwater beneath the peat was artesian. On steeper hillslopes, soils were drier and the water table was generally deeper (0.5 to 1 m below ground level), though the profile could fully saturate and groundwater levels reach the surface during the wettest period. Groundwater in deeper wells typically showed an anti-clockwise hysteresis compared to stream flow, and peak levels typically lagged behind the stream by a few hours in the valley bottom and >1

day in the upper hillslope. In contrast, shallower wells in the soil profiles in the riparian area showed more a responsive perched groundwater system with transmissivity feedback in the upper soil layers resulting in much more rapid responses which generally peaked before the stream and exhibited clockwise hysteresis. Analysis of stable isotopes in precipitation, groundwater and streamflow, indicated that groundwater was remarkably well mixed with limited fractionation effects, inferring precipitation on the upper, unconfined hillslopes was the dominant source of recharge - particularly during the winter. The study shows that groundwater plays two roles in generating stream flow: a constant baseflow supply to the stream and time varying-exfiltration into the edge of the riparian zone, which contributes to surface runoff during storm events.

Key words: groundwater, runoff, isotopes, hysteresis

1. Introduction

Climate change projections for the northern latitudes generally point to increased summer temperatures, and warmer, wetter winters which will probably also increase extreme rainfall events (Haddeland et al., 2014; McMichael et al., 2006; Taylor et al., 2013; UK Climate Projections (UKCP09)). These changes are likely to impact the dynamics of hillslope hydrology and the flow regime of affected catchments (Capell et al., 2014) causing a seasonal shift in runoff distribution towards reduced summer base flows and increased winter storm flows (Taylor et al., 2013; UKCP09) which may well increase flood risk (Arnell and Gosling, 2016). Further, warmer temperatures at higher latitudes in the boreal region are likely to result in less snow accumulation, earlier melting of the snow pack and more winter precipitation in form of rain and/or increased rain on snow runoff events (Tetzlaff et al., 2013). These changes in precipitation will have cascading effects in catchment systems, affecting the spatial and temporal patterns of soil moisture dynamics and groundwater recharge, which in turn will affect runoff generation processes (Kløve et al., 2014; Taylor et al.,

2013). These effects will be regionally variable according to different hydroclimatic and catchment characteristics (Capell et al., 2013). To better understand the likely implications we need direct observation of the hydrological behaviour of catchment hillslopes during the sort of extreme events that are expected to become more common (Taylor et al., 2013; Wilby et al., 2008, 2009).

Our limited understanding of hillslope response during extreme events reflects the short-term nature of most hillslope monitoring (typically limited to 1-2 years) which is usually insufficient to capture uncommon events. Also, most extreme events occur in unmonitored regions; and/or equipment damage or malfunction is more likely during such conditions (Marchi et al., 2010). Floods are the result of the superimposition of rapid runoff generating processes on wet catchments during extreme rainfall or snowmelt (Penna et al., 2013; Winter et al., 1998). The magnitude and severity of a flood event is usually highly dependent on antecedent hydro-meteorological conditions, as well as the event characteristics themselves. Multiple studies have linked pre-event soil moisture conditions to flood generation (Marchi et al., 2010; Nied et al., 2014; Nikolopoulos et al., 2011; Penna et al., 2011) implying limited available storage for incoming event inputs (Geris et al., 2015). Modelling work suggests that peak discharges and runoff volumes can be twice as high for near saturated initial conditions compared to dry conditions (Nikolopoulos et al., 2011). In addition, in humid environments, soil moisture conditions are often closely linked to groundwater (GW) levels in hillslope-riparian systems (Haria and Shand, 2004). When GW levels in saturated riparian areas rise above the ground surface, additional rain contributes directly to generation of saturation overland flow as described in variable source area theory (Dunne et al., 1975; McDonnell, 2003) and various case studies (Blumstock et al., 2015; McDonnell, 2003; Nippgen et al., 2015; Penna et al., 2011). If hillslopes become similarly saturated, the threshold change in connectivity often results in a non-linear increase in runoff response (Tetzlaff et al., 2014). Despite this, flood forecasting often focuses

on black-box rainfall-runoff models and rarely incorporates physically-based models of hillslope dynamics during extreme events (Penna et al., 2013).

Understanding GW dynamics and the associated connectivity between hillslopes and streams is fundamental to projecting catchment rainfall-runoff responses in extreme events. Catchment GW dynamics usually exhibit spatial organisation that is related to the landscape position relative to the stream network (Haught and Van Meerveld, 2011; Seibert et al., 2003). Numerous studies have reported close coupling between GW dynamics in riparian areas close to the channel network and stream flow response (e.g. Blumstock et al., 2016; Jencso et al., 2009; Seibert et al., 2003). This relationship can weaken with increasing distance from the streams (Seibert et al., 2003) and is modulated by hydroclimatic conditions, with antecedent wetness, rain event magnitude and intensity influencing the connectivity and response times between hillslopes and streams (Detty and McGuire, 2010a, 2010b; Penna et al., 2011; Tromp-van Meerveld and McDonnell, 2006a, 2006b). For example, Dahlke et al. (2012) found that during storm events with dry antecedent conditions, deeper GW contributed 33-71% of the total discharge. During wet antecedent conditions, the contribution of near-surface runoff sources was higher. Similarly, Tetzlaff et al. (2014) inferred limited hillslope GW response to small storm events. Only in larger events with elevated water tables did hillslope GW systems connect to riparian areas delivering storm runoff.

Riparian zones usually receive drainage from upslope areas and are often quasi-permanently saturated due to retentive organic soils (Capon et al., 2013; Grabs et al., 2012). They can form important habitats for biodiversity with vegetation communities adapted to the water-logged conditions (Banner and MacKenzie, 1998; González et al., 2016; SEPA, 2009). The riparian environment is usually characterised by a regular exchange of water and nutrients at the interface

between soil water, GW and streams (Bergstrom et al., 2016; Payn et al., 2009; Smart et al., 2001). Studies quantifying net gains and losses along stream channels (Covino and McGlynn, 2007; Somers et al., 2016) have shown that during drier conditions, older, deeper GW seeps from the riparian zones into the stream channels. With increasing wetness, hillslopes and streams become more strongly connected hydrologically (Jencso et al., 2009; Zimmer and McGlynn, 2017) and contributions of younger, shallower GW increase (Ala-aho et al., 2017; Gabrielli et al., 2012). Other studies have examined the role of deeper, bedrock GW on rainfall-runoff responses. Gabrielli et al. (2012) investigated two hillslopes, one in the Maimai catchment (New Zealand) and one in the H.J. Andrews Experimental Forest (USA, Oregon). At both sites, bedrock GW was an extremely dynamic component. Using data from the Panola Mountain Experimental hillslope in Georgia (USA), modelling by Ameli et al. (2015) also suggested that the hillslope storm response is less dependent on soil depth and more on the underlying bedrock permeability.

The field monitoring that is necessary to understand hillslope GW dynamics can be challenging in many headwater catchments as rugged, high altitude terrain with limited accessibility restricts possibilities, especially when it comes to drilling. Often, it is impractical and too expensive to use heavy drilling equipment for the installation of large numbers of boreholes, which are necessary to capture the high level of heterogeneity in the subsurface (Gabrielli and McDonnell, 2012). Consequently, environmental tracers have become important tools in catchment hydrology, offering indirect insights into the dynamics of surface and subsurface waters (Leibundgut et al., 2009; Soulsby et al., 1998). They are widely used to differentiate water sources, identify flow paths, investigate surface and subsurface mixing processes, and understand storage dynamics (Barthold et al., 2011; Lessels et al., 2016; Neal et al., 1997; Soulsby et al., 2005, 2004; Tetzlaff and Soulsby, 2008). Stable water isotopes of Deuterium and 18-Oxygen are particularly useful for identifying sources, pathways and the age of runoff sources (Kendall and McDonnell, 1998) and are now inexpensive to analyse.

Compared to the isotopic composition of local precipitation, stream samples depleted in heavier isotopes may be indicative of GW sources (from winter recharge) and enriched samples can be indicative of evaporative fractionation or summer rainfall (Kendall and McDonnell, 1998; Soulsby et al., 2007). Especially in low-temperature environments, the isotopic composition of natural waters is exclusively affected by physical processes, namely by phase changes (evaporation, condensation and melting) above or near the ground surface, as well as mixing at or below the ground surface (Leibundgut et al., 2009).

In this paper, we report the dynamics of an experimental hillslope where GW and soil moisture were monitored in the Bruntland Burn, an intensively studied experimental catchment in the Scottish Highlands. Crucially, the 13 month period included an extreme flood event with a >200 year return period (Marsh et al., 2016). Over the winter of 2015/16, parts of the northern UK experienced some of the highest river levels and worst flooding in over 100 years of hydrometric monitoring (Marsh et al., 2016; Soulsby et al., 2017). This resulted from unusually mild conditions in December, at a time when rainfall at high altitude normally falls as snow. Previous field and modelling work in the catchment has emphasised the importance of the extensive riparian wetlands as the dominant source of runoff (Tetzlaff et al., 2014). GW exfiltration provides both a major source of water to these wetlands throughout most of the year, as well as direct fluxes into the channel network to sustain the low flows (Ala-aho et al., 2017; Birkel et al., 2014, 2011a). GW also provides a large store of water that mixes with incoming precipitation to affect the attenuation and lag observed in isotopic signatures in stream water compared to precipitation (Soulsby et al., 2015). However, our understanding of GW dynamics at the hillslope-riparian interface is still limited, in particular during the extreme wetness conditions that were monitored during the study period and are expected to become more common (Blumstock et al., 2016). Therefore, this paper aims to answer the following specific questions:

(1) How does the hillslope GW respond to an extreme event in the context of more general variation over the year?

(2) How does the hysteresis of GW response in relation to the stream help us to understand how GW dynamics control hillslope – riparian zone connectivity during storm events?

(3) How do stable isotopes add to our understanding of GW dynamics at the hillslope-riparian zone interface?

2. Study site

The study was focused around a representative hillslope transect within a long-term experimental headwater catchment, the Bruntland Burn (3.2 km^2, Figure 1) in the Cairngorms National Park, NE Scotland. More detailed descriptions of the catchment can be found elsewhere (e.g. Birkel et al., 2011b, 2010; Blumstock et al., 2015; Soulsby et al., 2007). The local climate is transitional between temperate and boreal with a moderating maritime influence. Annual average air temperature is around 6 ^oC, with a daily average of 1 ^oC and 12 ^oC during winter and summer, respectively. The annual precipitation (P) of ~ 1100 mm (for period 2011 – 2016) is evenly distributed throughout the year and only ~ 5 % generally falls as snow. In colder years, this can exceed 10 %. Around half of the annual rainfall occurs during frequent, but low intensity events < 10 mm d^{-1}, and 75 % of the rain comes in events <20 mm d^{-1}. The total potential evapotranspiration (ET) and runoff (R) during the course of a year are around 400 mm and 700 mm, respectively (Birkel et al., 2011a). The average daily discharge is about 1.5 mm d^{-1}. It has been estimated that 25 – 35 % of the annual discharge is sustained by GW (Birkel et al., 2011a, 2011b).

The highest parts of the catchment reach 540 m a.s.l. and steep hillslopes fall towards a wide flat valley bottom at about 238 m a.s.l. reflecting the site's glacial history. The hillslope gradients reach 61^o, but have an average of ~14^o. The valley is also asymmetrical with steeper gradients on northern

slopes and gentler on the south. The granite-dominated bedrock with associated metamorphic rocks is overlain by extensive low-permeability glacial drift deposits, which cover about 65% of the catchment. The deposit reaches a depth of ~40 m in the valley bottom. In the riparian area, the drift is confined beneath the peat due to the slowly permeable deeper soil layers and covers most of the north-facing hillslope, where monitoring was focused (Figure 1a). The steeper hillslopes are covered by thinner (<5 m) lateral moraine and ice marginal deposits (Soulsby et al., 2016). Heather vegetation (*Calluna vulgaris*) dominates the hillslopes while *Sphagnum spp.* mosses and grass (*Molinia caerulea*) dominate the riparian areas. The catchment is mostly uncultivated land which is extensively managed. Only 11 % of the catchment area is covered in forest consisting mainly of Scots Pine (*Pinus sylvestris*).

The hydrological regime is flashy with responsive shallow GW levels (Blumstock et al., 2016; Tetzlaff et al., 2014). The riparian zone is characterised by organic peaty soils (usually ~1.5 m deep; Figure 1c). The landscape position and highly retentive nature of these soils result in quasi-permanent saturation of the valley bottom. This is sustained by GW seepage from the upper parts of hillslope. The GW table in the riparian zone is usually within 20cm of the ground surface and is usually highly responsive to precipitation events generating saturation overland flow (Soulsby et al., 2015). The extent of the saturation is a dynamic variable source area and can range from 2 – 40 % of the catchment area, depending on the antecedent wetness (Birkel et al., 2011b). Even small precipitation events trigger lateral flow generating saturation overland flow directly into the stream (Blumstock et al., 2016; Geris et al., 2015).

The lower footslope is a transitional area between the riparian zone and the upper hillslope. The peaty gley soils have a shallow (30 cm deep) peat horizon overlying a less permeable mineral subsoil. Similar to the riparian soils, the peaty gleys usually also have shallow GW tables and little storage

capacity and precipitation events initiate lateral flow (Tetzlaff et al., 2014). Shallow GW levels in the footslope exhibit similar behaviour to the riparian zone, being close to the surface and responsive to rain with high water levels triggering shallow lateral flow and saturation overland flow (Blumstock et al., 2016). However, they display a more marked GW table drawdown during drier periods (Geris et al., 2015).

The steeper upper hillslopes are dominated by more freely draining podzols, which display distinct wetting and drying cycles. During storm events, the wetting front moves rapidly through the soil profile with preferential flows via macropores in the root zone (Tetzlaff et al., 2014). The upper hillslope mostly drains vertically to GW recharge, but lateral flow occurs when the organic rich upper horizons become saturated (Geris et al., 2015). The GW levels are more variable in upslope areas falling into the drift (< -1 m) during dry spells and rapidly rising during wet periods into the soil profile. During very wet periods with continuous high water levels, shallow lateral flow connects the upper slopes to the stream (Blumstock et al., 2016; Tetzlaff et al., 2014).

3. Data and Methods

Between 1st August 2015 and 30th September 2016, rainfall was recorded (every 15 mins) using a tipping bucket gauge connected to a CR800 Campbell logger (resolution of 0.2 mm). The stream stage height was recorded at the catchment outlet, using an Odyssey capacitance probe (resolution of 0.8 mm). Stream flow was derived from a stage-discharge rating curve which was updated by regular gauging. An automatic weather station (AWS) is located in the NW of the catchment and the stage recorder is located at the outlet (Figure 1a). We also sampled daily precipitation and stream water for stable isotope analysis using an automated sampler unit (ISCO 3700) located near at the

catchment outlet. Paraffin was applied to the sample bottles inside automated sampler units to protect the water samples from evaporation.

A broadly representative hillslope transect was divided into three main hydropedological units: the peatland riparian zone in the valley bottom, the peaty gleys in the lower footslope and the podzols on the upper hillslope (Figure 1c). In each, we monitored water level dynamics of GW in shallower and deeper wells, the volumetric soil moisture content in the different soil horizons and stable isotope dynamics in the wells. The hillslope (Figure 2) starts in the riparian zone at 250 m and reaches up to about 290 m a.s.l. with an average slope of 6.1^{o} and a maximum of 20^{o}. The geology is granite bedrock overlain by glacial drift deposits; the drifts increase in thickness from around 5m on the upper slopes to ~25 m in the valley bottom (Soulsby et al., 2016).

The inaccessibility of the study site for heavy drilling equipment restricted us to the use of a portable handheld drill. In addition, the unconsolidated sandy matrix of the glacial drift deposits limited the depths and number of boreholes for the deeper wells. Upon reaching the drift layer, the water needed to cool the drill compromised the integrity of the borehole walls leading to their collapse when removing the corer to extract the soil. However, using a handheld petrol powered drill developed by Gabrielli and McDonnell (2012) we managed to establish four deeper wells (DW 1 – 4) on the monitored hillslope (Figure 2). The four boreholes range in depth from 160 cm up to 330 cm, reaching into the upper layer of the drift deposit (Table 1). The wells were cased with white PVC piping with an outside diameter of 2.2 cm and a 30 cm long screening section at the submerged end. We back-filled the space between borehole wall and well with clean gravel. After the screened section was fully covered by the gravel, we sealed the remaining space using bentonite. The shallower wells (ShW I-III) were drilled using a hand-auger and completed with fully screened white

PVC casing with a diameter of 3.7 cm. Their depths varied between 63 and 90 cm below the surface and remained within the soil profile (Table 1).

In each well, water levels were logged every 15 minutes. The shallower wells were fitted with the same Odyssey capacitance loggers as the stream gauge. The deeper wells were fitted with a Van Walt Ltd micro-diver. The diver measured the pressure of the water column (precision ±1.0 cm, resolution 0.2 cm) and the water temperature in the well (precision ±0.1 ^{o}C, resolution 0.01 ^{o}C). The diver measurements were corrected for air pressure using a BaroDiver located at the weather station (precision of ±0.5 cm and resolution of 0.1 cm). We used a manual dip meter to measure the GW level to verify the recorded data and correct any offsets. The GW levels are reported as depth to water table from the ground surface, with negative and positive values indicating the distance of GW table to the surface either below or above the surface, respectively.

The volumetric soil moisture content (vsmc) was measured every 15 min using Campbell time-domain reflectometer (TDR) probes connected to a CR800 Campbell logger. The TDR probes and duplicates (~2 m apart) were deployed at the depth of 10 cm, 30 cm and 50 cm in representative profiles of the main soil units near DW 2, DW 3 and DW 4 (Figure 2).

When possible, the deeper wells were sampled for stable isotopes every month and the shallower wells were sampled on seven occasions. The depth of well ShW III was around -47 cm below the soil surface and was dry during most of the study (~ 207 days), apart from larger storm events. This well was only sampled twice. Water was extracted from the wells using a battery power vacuum pump. Usually, two hours prior to the sampling the wells were pumped and allowed to recover. However,

during cold winter periods the upper part of the well was frozen preventing sampling on several occasions.

To prevent fractionation of samples during transport to the laboratory, they were collected in a 250 ml PVC bottle without headspace and then refrigerated. For analysis, we used a Los Gatos IWA-35d-EP Laser Spectrometer (precision of ±0.3 ‰ for ^{2}H; ±0.1 ‰ for ^{18}O) using standard protocols and calibrated to Vienna Standard Mean Ocean Water (VSMOW). The results are reported in δ notation.

The line-conditioned excess (lc-excess) (Landwehr and Coplen, 2006) was used to identify any evaporative fractionation (-ve values) of samples or moisture source differences (+ve values):

$$lc - excess = \delta^{2}\mathrm{H} - 7.7 * \delta^{18}\mathrm{O} - 4.9 \qquad \text{(Eq. 1)},$$

using the slope and intercept coefficient from the local meteoric water line (LMWL) for the catchment.

Hysteresis loops are simple but provide useful perspectives on the relationship between stream discharge and GW during storm events (Allen et al., 2010; Fovet et al., 2015; McGlynn et al., 2004). The rotational direction of the loop indicates if the y-axis component lags behind the x-axis component or if the y-axis component responds faster. We used hysteresis plots and cross-correlation to investigate these relationships based on the 15 minute data. The cross-correlation analysis and additional data processing was carried out with the R statistics program (version R 3.4.3); the cross-correlation used the function ccf() (R Core Team, 2017). For 13 rainfall events of different size, intensity and antecedent conditions were assessed using the normalized discharge and GW levels inside the different wells. A hysteresis index was calculated for each well during the

events to compare the size and shape of the hysteresis loops. We adapted the hysteresis index (HI_{LL}) of Lloyd et al. (2016). This is suitable for complex loops such as "figure-of-eight" scenarios as it does not simply consider the mid-point of discharge like the alternative HI_{LA} (Lawler et al., 2006). The HI_{LL} represents the average of all differences between rising and falling limb of GW level and the hysteresis corresponding to the different percentages of discharge. The discharge (Q) and the GW table (WT) were normalized for each individual storm event as follows:

$$Normalized\ Q_i = \frac{Q_i - Q_{min}}{Q_{max} - Q_{min}} \qquad \text{(Eq. 2)},$$

$$Normalized\ WT_i = \frac{WT_i - WT_{min}}{WT_{max} - WT_{min}} \qquad \text{(Eq. 3)},$$

Where Q_i and WT_i is the discharge and the GW table at time step *i*; $Q_{min/max}$ and $WT_{min/max}$ are the limits of discharge and the GW levels during the event. For each hysteresis loop, we calculated HI_{LL} every 5% of the normalized storm discharge (x-axis) and averaged the resulting 19 values to characterize the respective event (Lloyd et al., 2016). The HI_{LL} was calculated as follows:

$$HI_{LL} = WT_{RL\_norm} - WT_{FL\_norm} \qquad \text{(Eq. 4)}.$$

where WT_{RL_norm} and WT_{FL_norm} are the normalized GW levels of the rising (RL) and falling limb (FL) for the respective increments of normalized discharge. The values for the HI_{LL} can range from -1 to 1 with negative and positive values indicating anti-clockwise and clockwise behaviour, respectively. The numeral of the HI_{LL} represents the surface area of the hysteresis loop with high numbers indicating "wide" loops. For complex loops such as figure-8-loops, we used a weighted average of the HI_{LL}. Weighting was done by the proportion of the storm event the hysteresis is in an anti-clockwise phase against the proportion of when it is in a clockwise phase. If the larger proportion of the hysteresis is in a clockwise phase, the overall direction of the hysteresis will be classified as clockwise.

4. Results

4.1 Hillslope response to extreme hydroclimatic conditions

During the 13 month study period, precipitation totalled 1102 mm, which is close to the long-term average. Most of the rain fell during low intensity events (Figure 3a). However, unusual for a site where rainfall is normally quite evenly distributed, more than one-third of the total precipitation fell in a 46 day period. Between 1st December 2015 and 15th January 2016 this totalled 375 mm of rain, and resulted in the highest discharge and highest GW level recorded since monitoring in the catchment started in 2007, and the highest river flows in the region since 1829 (Marsh et al., 2016). During this period, the daily discharge exceeded 10 mm d^{-1} on twelve occasions with the highest recorded daily runoff total of 25.8 mm on 30th December 2015 (Figure 3a). On the same day, the precipitation was 56.7 mm d^{-1}. This period of high precipitation and discharge was followed by a comparatively dry day before an unusual sequence of 6 days where around 100 mm fell. The rest of the study period was characterised by relatively small events, with the exception of a wet period in June 2016 (Figure 2). A total of 99 days were without rain which equals a quarter of the study period. The lowest discharge was measured on the 27th August 2016 with 0.08 mm d^{-1}.

All wells in close proximity of the stream (DW 1, DW 2 and ShW I) shared a similar response to precipitation events and subsequent drying (Figure 3b and c). Due to logistical problems, ShW I was deployed three months into the study period. Similar to DW 1, the water level in ShW I was usually above the ground surface. At the beginning of the study period, the water level of DW 1 fluctuated more frequently between residing slightly above or below the ground surface. After DW 1, ShW I had consistently the highest recorded water levels of all wells. Even though DW 2 is less than 30 m away from DW 1 and ShW I, its water level was deeper and generally about 10 cm below the ground surface. The water level would rise several centimetres in response to rain events. These differences between DW 1 and DW 2 may indicate a valley asymmetry in the piezometric surface, with steeper hydraulic gradients on the northern side of the stream (Figure 1a). On the lower footslope, the

monitored water levels (DW 3 and ShW II) were deeper and mostly fluctuating between -20 to -30 cm below the ground surface. Water-level variations were still relatively damped. In the wells on the upper hillslope (DW 4 and ShW III), water levels were deepest at > 1 m below the ground surface. These wells showed the most dynamic responses to large rainfall events with rapid rises and declines of their water levels. The standard deviations for the water levels in DW 2, DW 3 and ShW I had fairly similar values of 7.1 cm, 7.2 cm and 7.6 cm, respectively. ShW II had the lowest standard deviation (4.7 cm) followed by DW 1 (5.7 cm), respectively. The wells on the upper slope displayed the highest standard deviations (DW 4 32 cm; ShW III 21.4 cm).

Larger storm events which brought much of the rainfall between the end of 2015 and start of 2016 caused the majority of the wells – except those on the lower footslope (ShW III and DW 3) – to display artesian behaviour (Figure 4). All other wells had their highest recorded water levels during that period. The deeper wells in the riparian zone (DW 1, DW 2) had their highest recorded water levels on 30th December 2015 – the day of the peak precipitation and discharge. The shallower well closest to the stream (ShW I) was lagging a few days behind, but held its highest water level for the duration of four days, starting on the 4th January 2016. On 4th January 2016, the deeper well on the lower footslope (DW 3) also recorded its highest water level, with -2.4 cm below the ground surface. This differed from ShW II, which had its highest reading of -15 cm on 30th December 2015 – similar to DW 1 and DW 2. On the upper hillslope, DW 4 and ShW III were the first wells during that time period to reach their highest water levels on the 24th December 2015, 6 days prior to the peak discharge. Their water levels plateaued at that level (±2 cm) for 22 days till the 14th January 2016. The water level then dropped rapidly after the 14th January 2016, disconnecting the upper hillslope from the stream network again.

During drier conditions, some wells shared the same date for their lowest reading, however, others varied. For example, the deeper wells closest to the stream had a month difference in their minimum water level with DW 2 on the 13th August 2015 and DW 1 on the 11th September 2015 with -20.4 cm and -4.3 cm, respectively. ShW I – which was not deployed in the field until late November 2015 – had its lowest reading with -12.5 cm on the 6th June 2016. At the lower footslope, DW 3 (-37.4 cm) and ShW II (-41.5 cm) had their lowest water level – like DW 1 – on the 11th September 2015. The water levels recorded on the upper hillslope were at their lowest point on 1st August 2016, -112.9 cm at DW 4). ShW III did not record water levels below - 47 cm and was dry half of the study period.

Water temperature (Figure 3d) was only recorded in the deeper wells. Water temperatures inside DW 1 and DW 2 showed low variability and were almost constant with values of around 7.5 °C. Water temperature in DW 3 on the lower footslope had a range of 6.4 °C between the extremes. The deeper well furthest away from the stream, DW 4, was slightly less variable than DW 3 with water temperature between 9.4 °C and4.7 °C.

Soil moisture dynamics along the hillslope are shown in Figure 5b-d and were closely linked to the GW dynamics. The vsmc in the riparian zone showed a quasi-permanent saturated state throughout the year - only once did the vsmc in the O horizon (10 cm) drop below 0.79 - indicating little available storage capacity. A similar pattern was observed in the top soil (10 cm) of the lower footslope, which also reached its wettest state at the end of the winter like the riparian zone (Figure 5b and c). This variation was less pronounced in the mineral horizons at 30 cm and 50 cm depths (Figure 5b). At the upper hillslope, as with GW, the vsmc showed the most responsive dynamics with highest recorded values in the beginning of January 2016 during the extremely wet winter, shortly before equipment

failure (Figure 5d). The rapid, subsequent drying of the soil was briefly interrupted by a few small rain events (~10 mm d^{-1}) at the beginning of February 2016 and then continued with smaller alterations till mid-June 2016, where a larger storm (> 40 mm d^{-1}) caused rapid wetting across the soil profile on the upper hillslope. Between mid-December 2015 and early January 2016, when the majority of the large precipitation events occurred, the vsmc in the O horizon (10 cm) and in the B horizon (50 cm) was almost constantly increasing before rapidly decreasing with the cessation of the rainfall (Figure 4). The E horizon (30 cm) had a swift rise in vsmc similar to the O and B horizon, but remained relatively steady after reaching a threshold around 0.38.

4.2 Hysteresis dynamics

The hysteresis of the normalized discharge and depth to water table relationships were compared for the different wells during thirteen storm events (Figure 3, Table 2). The length of the events ranged from less than a day up to eight days, though most lasted for about two to three days. Due to the exceptional nature of the overall Dec/Jan event, this period is considered separately below. Most events had initial discharge (Q_{pre}) below the daily mean of 0.08 $m^3 s^{-1}$ (though E3 and E5 were exceptions). The lowest initial discharge occurred in E8 and E9. The highest discharge peak (Q_{max}) occurred during E5 (1.12 $m^3 s^{-1}$ and an isolated peak in the wet Dec/Jan period) which also had the wettest antecedent conditions seven days prior to the start of the event (P_7)with a total sum of 142 mm of precipitation. Driest antecedent conditions were before E6, which also had the lowest precipitation. The highest amount of total rainfall with 70.2 mm was recorded during E9.

The hysteresis relationships between discharge and water levels varied between wells and events, but there were consistent patterns, with the deeper wells usually always exhibiting an anti-clockwise hysteresis loop, with the GW levels usually being higher during the falling limb of the hydrograph

(Table 3 and Figure 6, 7). A notable exception was DW 1 and DW 2 during E5 which probably reflected the recession of stream levels from the major rainfall in late December 2015 and early January 2016 (Table 3). During that event, all wells in the riparian zone had very narrow hysteresis loops and the records of ShW I were most likely affected by the higher stage height of the stream (i.e. surface water response). Shallower wells I and II predominantly experienced clockwise hysteresis loop directions (Table 3) in contrast to ShW III, presumably reflecting the effect of perched water tables and generation overland flow in the upper peaty soil horizons, rather than the response of deeper GW in the drift.

The majority of the wells were characterised by relatively small absolute HI_{LL} values below 0.5 (Table 3), representing relatively narrow hysteresis loop shapes, with only DW 3 and DW 4 exceeding this on five occasions (Table 3). This likely reflects the wet conditions of the soils in riparian and lower slope areas and the high-standing water table for most of the year. Whereas on the upper slope, the variation in water table response was one or two orders of magnitude greater. During all events, ShW I stood out with its consistent, narrow figure-of-eight loops (see examples in Figures 6, 7). The only two other wells displaying similar narrow figure-of-eight loops were the two deeper wells (DW 1, DW 2) in the riparian area during E4 and E5 which were respectively a large event in mid-December 2015 and the last event peak at the end of the wettest December/January period.

Table 3 also shows the peak-to-peak lag times during the events analysed; positive values indicate the GW levels peaking after the stream, and negative values indicate the GW peaking before the stream. Again, there was variation between events and sites, but some general patterns emerged. For most events, the deeper wells peaked after the stream, reflecting the slower response of the deeper GW system in the drift deposits. In contrast to the shallower wells, ShW I and ShW II, their

GW level peak preceded the stream, consistent with the clockwise hysteresis. In the deeper wells in the riparian zone DW 1 on average peaked some 5 hours before DW 2. For both sites there was a general, though inconsistent tendency for the lags to increase with drier antecedent conditions. DW 1 and ShW I usually had similar lags with small variations of < ± 2 h, though at ShW I the lag time was negative in all but one event. These short lag times are reflected in the steep GW response on the hydrographs rising limbs in the hysteresis plots for DW 1 and ShW I (Figures 6, 7). On the lower footslope, the shallower well ShW II peaked usually about 2-3 h before the stream, similar to ShW I. Time to peak was longer in deeper GW in the footslope; DW 3 peaked on average 16 h after the stream and the largest lag time occurred following E9 (a large event with dry antecedent conditions) with 41.25 h. The upper slope (DW 4, ShW III) usually displayed the largest lag times for both the deeper and shallower wells, where the mean time to peak was on average around a day after the event. In DW 4 the lag following E9 was 2.5 days, indicating much more gradual GW flow from the upper hillslopes. The lag times that optimized correlation between water levels in each well and the stream flow for the entire study period are given in Table 4a showing a broadly similar picture to the results from the event-based assessment (Table 4b).

Figure 8 shows the hysteresis patterns over the week-long extreme event in December/January. In such extreme wetness conditions at DW 1 and DW 2, the response is almost linear, apart from at the major event peak where surface saturation was extensive. In ShW I, this transition was more threshold-like. DW 3 showed more regular anti-clockwise loops, whilst ShW II showed more regular clockwise responses (Table 3). At DW 4 and ShW III the response was very threshold-like once surface saturation occurred. The lag times in the wells were noticeably reduced in the large Dec/Jan event, especially for the deeper wells (Table 4b).

Soil moisture variations along the transect matched the GW dynamics. The soils close to the stream were at or close to saturation during all thirteen events with no change in vsmc (Table 5); this dictated that in the riparian zone and lower footslope, very few events resulted in a hysteresis between soil moisture responses and stream flow (Table 6). Only E9, with the driest antecedent conditions showed a hysteretic response in soil moisture in the riparian zone, with a marked hysteresis loop (HI_{LL} = -1) as soil moisture re-wetted. On the lower footslope in the peaty gley, only the O horizon (upper 10 cm) registered substantial changes in vsmc during eight out of the thirteen events. Hysteresis could be clockwise or anticlockwise and response times were variable, with O horizon peaking up to 5 h before or 4 h after steam flow. The podzol soil profile on the steep slope furthest from the stream showed the greatest variability in soil moisture during storm events. The O horizon (10 cm) almost always had the largest change in vsmc during events, and peak soil moisture usually preceded stream flow (on average by 2 h). The response could be either clockwise or anti-clockwise, depending upon antecedent conditions and event characteristics, though the generally low HI_{LL} indicated narrow hysteresis loops. Soil moisture in the E horizon at 30 cm consistently displayed anti-clockwise loops with soil moisture higher on the falling limb and mostly peaking ~2h before the stream. The B horizon (50 cm) usually had the lowest vsmc and its hysteresis had mostly an anti-clockwise direction taking a figure-of-eight shape (Table 6). The B horizon also tended to reach its highest vsmc 3 h before the stream flow peaks. Overall, the soil moisture monitoring was less sensitive and informative than the GW levels as rapid, transient changes in water storage via water moving in macropores were not detected.

4.3 Dynamics in stable isotopes

Figure 9 summarises precipitation, GW and stream samples plotted in dual isotope space. Naturally, precipitation samples (inset of the Figure) showed the widest range, giving a local meteoric water line (LMWL) close to the global meteoric water line (GMWL). The stream water samples plotted in a

much narrower range (with the variation reduced by a factor of 10) and deviated from the LMWL, especially some enriched samples in the summer, indicative of evaporative fractionation (which is also shown by the negative lc-excess values in Figure 11c). The GW samples exhibit a narrower range than the stream with limited variability (See also Figure 10). They also plot in the same space as the more depleted stream samples. All the GW samples plotted close to GMWL and LMWL and showed no evidence of fractionation. This is also indicated in the positive lc-excess values in Figure 10.

Over the study, the signal for both isotopes (δ^2H and $\delta^{18}O$) in precipitation showed high variability and followed a general seasonal pattern with a tendency to more enriched values in summer and depleted values in winter, though day to day variability can be marked (Figure 11b; Table 7). The most enriched precipitation in δ^2H and $\delta^{18}O$ fell on the 10th June 2016 with -4.1 ‰ and -1 ‰, respectively and the most depleted rain fell in the beginning of December 2015 with -162.3 ‰ and -21.5 ‰ respectively. The isotope signal of the precipitation which caused the extreme discharges during mid-December 2015 and early January 2016 was surprisingly enriched for winter and close to the long-term mean (Figure 4d).

The range of stream water signal was much more damped than that of precipitation (Figure 11b; Table 7), though the main anomalies in the stream water signal were driven by the variability of input. As a result, the lack of variation in the rainfall signal in the wet December/January period gave a limited stream isotope response, until precipitation became depleted in the final few days of the wettest sequence. Some stream water samples in early December were more depleted than any ground water samples. Although the lc-excess of precipitation was highly variable (Figure 10c), apart from a few exceptions, the lc-excess in the stream water was consistently above zero, limiting

evidence for the influence of evaporative fractionation effects to brief periods in the summers of 2015 and 2016.

Figure 10 shows the boxplots for all stable water isotopes measured in the wells over the study period. Given that the deeper wells were sampled at approximately monthly intervals (and the shallow wells on seven occasions), the isotope composition was remarkably consistent. DW 2 in the riparian zone had marginally more enriched compositions compared to DW 1 and ShW I, which both showed a similar mean and range. As for the lower footslope, the shallower well ShW II had slightly more enriched values than DW 3. DW 4, on the hillslope top, displayed the largest range in δ^2H and was the most depleted of the deeper wells. Overall, compositions in DW 2 and DW 3 were slightly more enriched than in DW 1 and DW 4.

5. DISCUSSION

5.1 Hillslope response in large events

Monitoring showed the dominance of the wet 9 day period at the turn of 2015/16 in shaping the hydrological regime during the study year. Indeed, most other precipitation events were quite small and the stream flow responses were relatively modest with the main exception of event 10 (E10) in June 2016 (Figure 3a). Insights from the data revealed new perspectives on the catchment hydrological functions under such extreme conditions, even though these were consistent with a general model of variable source area expansion in wetter conditions(cf. Dunne et al., 1975). For example, the GW data emphasises the unique, prolonged catchment wetness state during the late December/January period, with all wells apart from DW 3 becoming artesian (Figure 4b, c). This was broadly consistent with classic gravity driven Tothian flow models in porous media, resulting from rapid, high recharge in the upper catchment increasing pressure heads (Toth, 1963). The catchment

storage remained super-charged after the event and needed several weeks drainage before water levels subsided; even the upper hillslope of the transect at DW 4 retained a water table within a few centimetres of the soil surface for almost a month. With such high GW levels, and unusually extensive surface saturation, overland flow (saturation excess) was the dominant runoff process. This explains the very high runoff rates during this event resulting in a runoff coefficient of ~80% (Soulsby et al., 2017); much higher than those previously reported in the catchment for large events (~40% see Tetzlaff et al., 2014). This non-linearity of the rainfall-runoff response reflects the filling of almost all soil water and GW storage in the catchment with each increment of rainfall increasingly displacing stored water as the event progressed. Our new process insights have implications for nature-based solutions to flood management that argue that increasing land cover of vegetation that "uses" more water, such as forestry, can help create storage deficits to mitigate heavy rainfall (e.g. Marshall et al., 2014). Here, in the largest winter floods, data show that such a strategy is unlikely to significantly reduce storm runoff (Soulsby et al., 2017).

In many ways, the underpinning runoff processes driving the hydrological response of the Bruntland Burn are consistent with other studies in upland catchments which have reported similar non-linearity in hillslope water fluxes as variable source areas expand and connectivity increases (Dahlke et al., 2012; Nippgen et al., 2015). Similarly, in a rather different setting of the free draining soils at the Panola catchment, Tromp-van Meerveld and McDonnell (2006a, 2006b) showed that high GW levels acted as threshold that regulated a transient, highly non-linear storm period response in terms of runoff generation. This is similar to the response observed in the upper hillslope at DW 4 here, and elsewhere (e.g. Detty and McGuire, 2010b; McGuire and McDonnell, 2010; Montgomery et al., 1997), where in most events precipitation replenishes soil moisture deficits or recharges GW. Likewise, in the Bruntland burn, only when the water table reaches the soil surface, as in the December/January event, does high connectivity occur as water can move laterally in the more

permeable soil horizons or moves as overland flow, as shown by Bishop et al. (2011) at Gardsjon in Sweden. Other studies have reported similar ability of increased connectivity of distant hillslopes driving non-linear runoff response in large events with wet antecedent conditions (e.g. Jencso et al., 2009; Sidle et al., 2000). Despite this non-linerarity in hillslope response, the importance of the saturated peat soils in driving the runoff response of smaller events has been stressed before at the study site (Tetzlaff et al., 2014). In these situations, the water table is already close to the surface modulating the influence of larger events, as hillslope waters drain through and over the riparian zone. Similar runoff mechanisms have been identified in other northern boreal catchments similarly influenced by riparian peatlands (e.g. Laudon et al., 2007).

5.2 Insights from hysteresis relationships between groundwater and streamflow responses

Plotting hysteresis relationships between GW levels and streamflow responses in storm events (Figures 6-8) provides richer insights into the mechanisms of runoff generation. The generally consistent anti-clockwise nature of the hysteresis loops in the deeper wells contrasted with the clockwise loops in the shallow wells ShW I and ShW II in the valley bottom. This underlines the integrated nature of the topographically-driven GW-surface water interactions in the catchment. This integrates a deeper, slower responding GW flow system in the deeper drift that lags behind the stream response, and shallower perched water table responses in the valley bottom peat soils where the deeper peat acts as an impermeable layer maintaining perched water tables in the peat, and confining deeper GW in the drift (Ala-aho et al., 2017). Moreover, the shallow flow system in the saturated area is maintained in part by GW exfiltration at the edge of the riparian zone (Tetzlaff et al., 2014). Thus, the saturated area typically responds 1-2 hours before the stream as overland flow and shallow lateral flow is generated by rainfall dominating the catchment response. In contrast, the deeper GW responds more slowly, especially on the upper hillslopes as GW flow from the interfluves moves laterally downslope. In the large event, these lags in the deeper flow system were shortened

as the more extensive saturation and higher hydraulic gradients resulted in greater connectivity. Variation in soil moisture data over time was too small to detect such hysteresis.

Other studies have reported similar differences of the hysteresis response with shallow GW in riparian areas responding more rapidly to the stream, whilst deeper hillslope GW lags behind (Fovet et al., 2015). More generally, the spatial differences in the lag of the GW response in the Bruntland Burn reflects the availability (or otherwise) of storage in the soils and GW systems which is high on the hillslopes and lower in the riparian zone. This is contrasting to other studies which show either anti-clockwise hysteresis in the hillslope response when the catchment is dry and clockwise when it is wet (e.g. Penna et al., 2011).

5.3 Stable isotopes in groundwater systems

The transformation of isotopes in rainfall – runoff processes in the Bruntland Burn catchment have been extensively studied (e.g. Birkel et al., 2011b; Soulsby et al., 2015; Sprenger et al., 2017; Tetzlaff et al., 2014). The results presented here show the same seasonality, damping and lagging of the rainfall signal in runoff previously reported (Figure 11), with GW being particularly well-mixed (Figure 10) and indicating the stronger influence of depleted winter precipitation in recharge (Scheliga et al., 2017). Unfortunately, anticipation that the wet December-January period would add new insights was confounded by the event precipitation having an isotope signal close to the long-term mean and not causing any major departure in the GW and stream water isotope signatures. Nonetheless, the higher contributions of "new" water implied were consistent with the higher runoff coefficients noted above. Earlier work by Birkel et al. (2015) examining longer-term (6 years) variation of isotopes in rainfall and runoff at the site showed that in some periods, low variability in precipitation isotopes can result in time series with low information content. Thus, unlike other

hillslope studies (Kabeya et al., 2007), stable isotopes were not especially discriminatory as tracers in GW in this particular. Partly this also reflects the large water volumes stored in the catchment peat soils and aquifers which can largely mix the rainfall signal effectively even in large events (Soulsby et al., 2016). Other studies have also reported similar time invariance of stable isotopes in hillslope GW where large mixing volumes are available (Oshun et al., 2016).

Despite such issues, some subtle new insights came from the isotopes data collected that help develop further a perceptual model of GW recharge in the catchment (Figure 12). This shows the dominant role of winter recharge on the catchment interfluves (indicated by the most depleted GW in deep wells DW 1 and DW 4) and the confined nature of the aquifer in the riparian zone close to the streams. Despite the riparian area soils and drifts being saturated, a shallower "perched" GW flow system occurs above the confining layers of the more impermeable peat layers below the acrotelm (i.e. the more permeable surface (~20 cm) horizons). This also explains the frequent occurrence of artesian conditions at DW 1 and DW 2. The valley asymmetry with the shorter, steeper hillslope on the north side of the stream likely explains the higher water table at DW 1, whilst the more depleted isotope signature here is consistent with more direct winter recharge from the exposed permeable bedrock in the northern upper hillslope. In contrast, the higher (i.e. more enriched) deuterium values at DW 2 and DW 3 are likely indicative of infiltration of water on the steeper and lower hillslopes that has slightly less depleted rainfall signatures, and possibly the influence of evaporated summer soil water which can affect recharge in this part of the catchment (Sprenger et al., 2017). However, if this is the case, the still high lc-excess values indicate that evaporation is modest.

5.4 Implications for monitoring

Monitoring such large events is largely an issue of serendipity, but the study here underlines the value of longer-term data sets at experimental sites to contextualise extreme events (Tetzlaff et al., 2017). This is reflected in the interpretation of the somewhat disappointing isotope data from December 2015 as mentioned above, and also in being able to understand the unusual GW responses. In terms of the more specific insights from monitoring, the quasi-permanently saturated riparian area in the Bruntland Burn illustrates the greater sensitivity of GW levels to the rainfall-runoff response compared to soil moisture data. Whilst riparian water table fluctuations showed sensitivity to almost all events, soil moisture was only sensitive to more seasonal changes and only reflected short-term variability in the upper hillslope. This presumably reflects the lack of short-term soil storage in the riparian area compared to the upper hillslope. Thus, whilst others have shown that runoff responses are highly sensitive to riparian soil moisture fluctuations (e.g Penna et al., 2015), GW is a more appropriate measurement at our site. That said, the upper hillslope soil moisture time series provides a good proxy for GW variations in this part of the catchment, as the profile is more freely draining with periods of soil moisture deficits and saturation depending on varying GW levels.

6. CONCLUSIONS

By monitoring hydrological conditions in a small experimental catchment in the Scottish Highlands, we were fortunate to monitor the wettest period and largest flood event in over 50 years of data record. The catchment became almost fully saturated with virtually no available storage capacity for the precipitation input. For a period of several weeks, the piezometric surface of much of the catchment was at or above the surface. The event amplified normal rainfall runoff processes, with extensive saturation overland flow from expanded variable source areas in riparian wetlands dominating the storm period response. However, this was mostly sustained by exfiltration from deeper GW flow systems, which interacted with incident rainfall to extend the saturation area,

driving a highly non-linear increase in the storm runoff response and a runoff coefficient of ~80%. We also found that monitoring water tables in GW is a more sensitive approach than soil moisture alone to understanding the storage-discharge relationships in upland catchments with extensive cover of saturated soils. This is because soil moisture is close to saturation for much of the year, and bulk soil moisture measurements are insensitive to the transient changes in wetness where overland flow and shallow subsurface flow paths in macropores dominate the storm response. The GW data also exhibit hysteretic relationships with streamflow, showing shallow perched riparian GW respond first and drive the rising limb of the hydrograph, whilst GW in deeper hillslope drifts sustain the recession limb. As isotope variations in event rainfall were close to the long-term mean of stream water in the large event, tracer monitoring provided little new insight into runoff processes, though it highlighted the importance of winter recharge on the upper hillslopes.

Acknowledgements

We would like to thank the European Research Council (ERC, project GA 335910 VeWa) for funding. We also thank Chris Gabrielli for his help with some of the initial deeper boreholes.

REFERENCES

Ala-aho, P., Soulsby, C., Wang, H., Tetzlaff, D., 2017. Integrated surface-subsurface model to investigate the role of groundwater in headwater catchment runoff generation: A minimalist approach to parameterisation. J. Hydrol. 547, 664–677. https://doi.org/10.1016/j.jhydrol.2017.02.023

Allen, D.M., Whitfield, P.H., Werner, A., 2010. Groundwater level responses in temperate mountainous terrain: regime classification, and linkages to climate and streamflow. Hydrol. Process. 24, 3392–3412. https://doi.org/10.1002/hyp.7757

Ameli, A.A., Craig, J.R., McDonnell, J.J., 2015. Are all runoff processes the same? Numerical experiments comparing a Darcy-Richards solver to an overland flow-based approach for subsurface storm runoff simulation. Water Resour. Res. 51, 10008–10028. https://doi.org/10.1002/2015WR017199

Arnell, N.W., Gosling, S.N., 2016. The impacts of climate change on river flood risk at the global scale. Clim. Change 134, 387–401. https://doi.org/10.1007/s10584-014-1084-5

Banner, A., MacKenzie, W., 1998. Riparian Areas: Providing Landscape Habitat Diversity Part 5 of 7, Biodiversity: Management Concepts in Landscape Ecology. Smithers.

Barthold, F.K., Tyralla, C., Schneider, K., Vaché, K.B., Frede, H.-G., Breuer, L., 2011. How many tracers do we need for end member mixing analysis (EMMA)? A sensitivity analysis. Water Resour. Res. 47. https://doi.org/10.1029/2011WR010604

Bergstrom, A., Jencso, K.G., McGlynn, B.L., 2016. Spatiotemporal processes that contribute to hydrologic exchange between hillslopes, valley bottoms, and streams. Water Resour. Res. 52, 4628–4645. https://doi.org/10.1002/2015WR017972

Birkel, C., Soulsby, C., Tetzlaff, D., 2015. Conceptual modelling to assess how the interplay of hydrological connectivity, catchment storage and tracer dynamics controls nonstationary water age estimates. Hydrol. Process. 29, 2956–2969. https://doi.org/10.1002/hyp.10414

Birkel, C., Soulsby, C., Tetzlaff, D., 2014. Integrating parsimonious models of hydrological connectivity and soil biogeochemistry to simulate stream DOC dynamics. J. Geophys. Res. Biogeosciences 119, 1030–1047. https://doi.org/10.1002/2013JG002551

Birkel, C., Soulsby, C., Tetzlaff, D., 2011a. Modelling catchment-scale water storage dynamics: reconciling dynamic storage with tracer-inferred passive storage. Hydrol. Process. 25, 3924–3936. https://doi.org/10.1002/hyp.8201

Birkel, C., Tetzlaff, D., Dunn, S.M., Soulsby, C., 2011b. Using time domain and geographic source tracers to conceptualize streamflow generation processes in lumped rainfall-runoff models. Water Resour. Res. 47. https://doi.org/10.1029/2010WR009547

Birkel, C., Tetzlaff, D., Dunn, S.M., Soulsby, C., 2010. Towards a simple dynamic process conceptualization in rainfall-runoff models using multi-criteria calibration and tracers in temperate, upland catchments. Hydrol. Process. 24. https://doi.org/10.1002/hyp.7478

Bishop, K., Seibert, J., Nyberg, L., Rodhe, A., 2011. Water storage in a till catchment. II: Implications of transmissivity feedback for flow paths and turnover times. Hydrol. Process. 25, 3950–3959. https://doi.org/10.1002/hyp.8355

Blumstock, M., Tetzlaff, D., Dick, J.J., Nuetzmann, G., Soulsby, C., 2016. Spatial organization of groundwater dynamics and streamflow response from different hydropedological units in a montane catchment. Hydrol. Process. 30, 3735–3753. https://doi.org/10.1002/hyp.10848

Blumstock, M., Tetzlaff, D., Malcolm, I.A., Nuetzmann, G., Soulsby, C., 2015. Baseflow dynamics: Multi-tracer surveys to assess variable groundwater contributions to montane streams under low flows. J. Hydrol. 527, 1021–1033. https://doi.org/10.1016/j.jhydrol.2015.05.019

Capell, R., Tetzlaff, D., Essery, R., Soulsby, C., 2014. Projecting climate change impacts on stream flow regimes with tracer-aided runoff models - preliminary assessment of heterogeneity at the mesoscale. Hydrol. Process. 28, 545–558. https://doi.org/10.1002/hyp.9612

Capell, R., Tetzlaff, D., Soulsby, C., 2013. Will catchment characteristics moderate the projected effects of climate change on flow regimes in the Scottish Highlands? Hydrol. Process. 27, 687–699. https://doi.org/10.1002/hyp.9626

Capon, S.J., Chambers, L.E., Mac Nally, R., Naiman, R.J., Davies, P., Marshall, N., Pittock, J., Reid, M., Capon, T., Douglas, M., Catford, J., Baldwin, D.S., Stewardson, M., Roberts, J., Parsons, M., Williams, S.E., 2013. Riparian Ecosystems in the 21st Century: Hotspots for Climate Change Adaptation? Ecosystems 16, 359–381. https://doi.org/10.1007/s10021-013-9656-1

Covino, T.P., McGlynn, B.L., 2007. Stream gains and losses across a mountain-to-valley transition: Impacts on watershed hydrology and stream water chemistry. Water Resour. Res. 43, 1–14. https://doi.org/10.1029/2006WR005544

Dahlke, H.E., Easton, Z.M., Lyon, S.W., Todd Walter, M., Destouni, G., Steenhuis, T.S., 2012. Dissecting the variable source area concept - Subsurface flow pathways and water mixing processes in a hillslope. J. Hydrol. 420–421, 125–141. https://doi.org/10.1016/j.jhydrol.2011.11.052

Detty, J.M., McGuire, K.J., 2010a. Threshold changes in storm runoff generation at a till-mantled headwater catchment. Water Resour. Res. 46, 1–15. https://doi.org/10.1029/2009WR008102

Detty, J.M., McGuire, K.J., 2010b. Topographic controls on shallow groundwater dynamics: implications of hydrologic connectivity between hillslopes and riparian zones in a till mantled catchment. Hydrol. Process. 24, 2222–2236. https://doi.org/10.1002/hyp.7656

Dunne, T., Moore, T.R., Taylor, C.H., 1975. Recognition and prediction of runoff-producing zones in humid regions. Hydrol. Sci. Bull. 20, 305–327.

Fovet, O., Ruiz, L., Hrachowitz, M., Faucheux, M., Gascuel-Odoux, C., 2015. Hydrological hysteresis and its value for assessing process consistency in catchment conceptual models. Hydrol. Earth Syst. Sci. 19, 105–123. https://doi.org/10.5194/hess-19-105-2015

Gabrielli, C.P., McDonnell, J.J., 2012. An inexpensive and portable drill rig for bedrock groundwater studies in headwater catchments. Hydrol. Process. 26, 622–632. https://doi.org/10.1002/hyp.8212

Gabrielli, C.P., McDonnell, J.J., Jarvis, W.T., 2012. The role of bedrock groundwater in rainfall-runoff response at hillslope and catchment scales. J. Hydrol. 450–451, 117–133. https://doi.org/10.1016/j.jhydrol.2012.05.023

Geris, J., Tetzlaff, D., McDonnell, J.J., Soulsby, C., 2015. The relative role of soil type and tree cover on water storage and transmission in northern headwater catchments. Hydrol. Process. 29, 1844–1860. https://doi.org/10.1002/hyp.10289

González, E., Felipe-Lucia, M.R., Bourgeois, B., Boz, B., Nilsson, C., Palmer, G., Sher, A.A., 2016. Integrative conservation of riparian zones. Biol. Conserv. https://doi.org/10.1016/j.biocon.2016.10.035

Grabs, T.J., Bishop, K., Laudon, H., Lyon, S.W., Seibert, J., 2012. Riparian zone hydrology and soil

water total organic carbon (TOC): Implications for spatial variability and upscaling of lateral riparian TOC exports. Biogeosciences 9, 3901–3916. https://doi.org/10.5194/bg-9-3901-2012

Haddeland, I., Heinke, J., Biemans, H., Eisner, S., Flörke, M., Hanasaki, N., Konzmann, M., Ludwig, F., Masaki, Y., Schewe, J., Stacke, T., Tessler, Z.D., Wada, Y., Wisser, D., 2014. Global water resources affected by human interventions and climate change. Proc. Natl. Acad. Sci. U. S. A. 111, 3251–6. https://doi.org/10.1073/pnas.1222475110

Haria, A.H., Shand, P., 2004. Evidence for deep sub-surface flow routing in forested upland Wales : implications for contaminant transport and stream flow generation. Hydrol. Earth Syst. Sci. 8, 334–344. https://doi.org/10.5194/hess-8-334-2004

Haught, D.R.W., Van Meerveld, H.J., 2011. Spatial variation in transient water table responses: Differences between an upper and lower hillslope zone. Hydrol. Process. 25, 3866–3877. https://doi.org/10.1002/hyp.8354

Jencso, K.G., McGlynn, B.L., Gooseff, M.N., Wondzell, S.M., Bencala, K.E., Marshall, L.A., 2009. Hydrologic connectivity between landscapes and streams: Transferring reach- and plot-scale understanding to the catchment scale. Water Resour. Res. 45, 1–16. https://doi.org/10.1029/2008WR007225

Kabeya, N., Katsuyama, M., Kawasaki, M., Ohte, N., Sugimoto, A., 2007. Estimation of mean residence times of subsurface waters using seasonal variation in deuterium excess in a small headwater catchment in Japan. Hydrol. Process. 21, 308–322. https://doi.org/10.1002/hyp.6231

Kendall, C., McDonnell, J.J., 1998. Isotope Tracers in Catchment Hydrology, 1st ed. Elsevier sciene, Amsterdam.

Kløve, B., Ala-Aho, P., Bertrand, G., Gurdak, J.J., Kupfersberger, H., Kværner, J., Muotka, T., Mykrä, H., Preda, E., Rossi, P.M., Uvo, C.B., Velasco, E., Pulido-Velazquez, M., 2014. Climate change impacts on groundwater and dependent ecosystems. J. Hydrol. 518, 250–266. https://doi.org/10.1016/j.jhydrol.2013.06.037

Landwehr, J.M., Coplen, T.B., 2006. Line-conditioned excess: a new method for characterizing stable hydrogen and oxygen isotope ratios in hydrologic systems, in: Isotopes in Environmental Studies - Aquatic Forum 2004. IAEA, pp. 132–135.

Laudon, H., Sjöblom, V., Buffam, I., Seibert, J., Mörth, M., 2007. The role of catchment scale and landscape characteristics for runoff generation of boreal streams. J. Hydrol. 344, 198–209. https://doi.org/10.1016/j.jhydrol.2007.07.010

Lawler, D.M., Petts, G.E., Foster, I.D.L., Harper, S., 2006. Turbidity dynamics during spring storm events in an urban headwater river system: The Upper Tame, West Midlands, UK. Sci. Total Environ. 360, 109–126. https://doi.org/10.1016/j.scitotenv.2005.08.032

Leibundgut, C., Maloszewski, P., Külls, C., 2009. Tracers in Hydrology. John Wiley & Sons.

Lessels, J.S., Tetzlaff, D., Birkel, C., Dick, J.J., Soulsby, C., 2016. Water sources and mixing in riparian wetlands revealed by tracers and geospatial analysis. Water Resour. Res. 52, 456–470. https://doi.org/10.1002/2015WR017519

Lloyd, C.E.M., Freer, J.E., Johnes, P.J., Collins, A.L., 2016. Technical Note: Testing an improved index for analysing storm discharge–concentration hysteresis. Hydrol. Earth Syst. Sci. 20, 625–632. https://doi.org/10.5194/hess-20-625-2016

Marchi, L., Borga, M., Preciso, E., Gaume, E., 2010. Characterisation of selected extreme flash floods

in Europe and implications for flood risk management. J. Hydrol. 394, 118–133. https://doi.org/10.1016/j.jhydrol.2010.07.017

Marsh, T.J., Kirby, C., Barker, L., Henderson, E., Hannaford, J., 2016. The winter floods of 2015 / 2016 in the UK - a review.

Marshall, M.R., Ballard, C.E., Frogbrook, Z.L., Solloway, I., Mcintyre, N., Reynolds, B., Wheater, H.S., 2014. The impact of rural land management changes on soil hydraulic properties and runoff processes: Results from experimental plots in upland UK. Hydrol. Process. 28, 2617–2629. https://doi.org/10.1002/hyp.9826

McDonnell, J.J., 2003. Where does water go when it rains? Moving beyond the variable source area concept of rainfall-runoff response. Hydrol. Process. 17, 1869–1875. https://doi.org/10.1002/hyp.5132

McGlynn, B.L., Mcdonnell, J.J., Seibert, J., Kendall, C., 2004. Scale effects on headwater catchment runoff timing, flow sources, and groundwater-streamflow relations. Water Resour. Res. 40, 1–14. https://doi.org/10.1029/2003WR002494

McGuire, K.J., McDonnell, J.J., 2010. Hydrological connectivity of hillslopes and streams: Characteristic time scales and nonlinearities. Water Resour. Res. 46. https://doi.org/10.1029/2010WR009341

McMichael, A.J., Woodruff, R.E., Hales, S., 2006. Climate change and human health: Present and future risks. Lancet 367, 859–869. https://doi.org/10.1016/S0140-6736(06)68079-3

Montgomery, D.R., Dietrich, W.E., Torres, R., Anderson, S.P., Heffner, J.T., Loague, K., 1997. Hydrologic response of a steep, unchanneled valley to natural and applied rainfall. Water Resour. Res. 33, 91–109. https://doi.org/10.1029/96WR02985

Neal, C., Hill, T., Hill, S., Reynolds, B., 1997. Acid neutralization capacity measurements in surface and ground waters in the Upper River Severn, Plynlimon: from hydrograph splitting to water flow pathways. Hydrol. Earth Syst. Sci. 1, 687–696. https://doi.org/10.5194/hess-1-687-1997

Nied, M., Pardowitz, T., Nissen, K., Ulbrich, U., Hundecha, Y., Merz, B., 2014. On the relationship between hydro-meteorological patterns and flood types. J. Hydrol. 519, 3249–3262. https://doi.org/10.1016/j.jhydrol.2014.09.089

Nikolopoulos, E.I., Anagnostou, E.N., Borga, M., Vivoni, E.R., Papadopoulos, A., 2011. Sensitivity of a mountain basin flash flood to initial wetness condition and rainfall variability. J. Hydrol. 402, 165–178. https://doi.org/10.1016/j.jhydrol.2010.12.020

Nippgen, F., McGlynn, B.L., Emanuel, R.E., 2015. The spatial and temporal evolution of contributing areas. Water Resour. Res. 51, 4550–4573. https://doi.org/10.1002/2014WR016719

Oshun, J., Dietrich, W.E., Dawson, T.E., Fung, I., 2016. Dynamic, structured heterogeneity of water isotopes inside hillslopes. Water Resour. Res. 52, 164–189. https://doi.org/10.1002/2015WR017485

Payn, R.A., Gooseff, M.N., McGlynn, B.L., Bencala, K.E., Wondzell, S.M., 2009. Channel water balance and exchange with subsurface flow along a mountain headwater stream in Montana, United States. Water Resour. Res. 45. https://doi.org/10.1029/2008WR007644

Penna, D., Borga, M., Zoccatelli, D., 2013. Analysis of Flash-Flood Runoff Response, with Examples from Major European Events. Treatise Geomorphol. 7, 95–104. https://doi.org/10.1016/B978-0-12-374739-6.00153-6

Penna, D., Mantese, N., Hopp, L., Dalla Fontana, G., Borga, M., 2015. Spatio-temporal variability of

piezometric response on two steep alpine hillslopes. Hydrol. Process. 29, 198–211. https://doi.org/10.1002/hyp.10140

Penna, D., Tromp-Van Meerveld, H.J., Gobbi, A., Borga, M., Dalla Fontana, G., 2011. The influence of soil moisture on threshold runoff generation processes in an alpine headwater catchment. Hydrol. Earth Syst. Sci. 15, 689–702. https://doi.org/10.5194/hess-15-689-2011

R Core Team, 2017. R: A language and environment for statistical computing. R Found. Stat. Comput. Vienna.

Scheliga, B., Tetzlaff, D., Nuetzmann, G., Soulsby, C., 2017. Groundwater isoscapes in a montane headwater catchment show dominance of well-mixed storage. Hydrol. Process. 1–16. https://doi.org/10.1002/hyp.11271

Seibert, J., Bishop, K., Rodhe, A., McDonnell, J.J., 2003. Groundwater dynamics along a hillslope: A test of the steady state hypothesis. Water Resour. Res. 39. https://doi.org/10.1029/2002WR001404

SEPA, 2009. Engineering in the Water Environment Good Practice Guide: Riparian Vegetation Management. East Kilbride.

Sidle, R.C., Tsuboyama, Y., Noguchi, S., Hosoda, I., Fujieda, M., Shimizu, T., 2000. Stormflow generation in steep forested headwaters: A linked hydrogeomorphic paradigm. Hydrol. Process. 14, 369–385. https://doi.org/10.1002/(SICI)1099-1085(20000228)14:3<369::AID-HYP943>3.0.CO;2-P

Smart, R., Soulsby, C., Cresser, M.S., Wade, A.J., Townend, J., Billett, M.F., Langan, S., 2001. Riparian zone influence on stream water chemistry at different spatial scales: a GIS-based modelling approach, an example for the Dee, NE Scotland. Sci. Total Environ. 173–193.

Somers, L., Gordon, R., McKenzie, J., Lauta, L., Wigmore, O., Glose, A., Glas, R., Aubry-wake, C., Mark, B., Baraer, M., Condom, T., 2016. Quantifying groundwater- surface water interactions in a proglacial valley, Cordillera Blanca, Peru. Hydrol. Process. https://doi.org/10.1002/hyp.10912

Soulsby, C., Birkel, C., Geris, J., Dick, J.J., Tunaley, C., Tetzlaff, D., 2015. Stream water age distributions controlled by storage dynamics and nonlinear hydrologic connectivity: Modeling with high-resolution isotope data. Water Resour. Res. 51, 7759–7776. https://doi.org/10.1002/2015WR017888

Soulsby, C., Bradford, J., Dick, J.J., McNamara, J.P., Geris, J., Lessels, J.S., Blumstock, M., Tetzlaff, D., 2016. Using geophysical surveys to test tracer-based storage estimates in headwater catchments. Hydrol. Process. https://doi.org/10.1002/hyp.10889

Soulsby, C., Chen, M., Ferrier, R.C., Helliwell, R.C., Jenkins, A., Harriman, R., 1998. Hydrogeochemistry of shallow groundwater in an upland Scottish catchment. Hydrol. Process. 12, 1111–1127. https://doi.org/10.1002/(SICI)1099-1085(19980615)12:7<1111::AID-HYP633>3.0.CO;2-2

Soulsby, C., Dick, J.J., Scheliga, B., Tetzlaff, D., 2017. Taming the Flood – how far can we go with trees? Hydrol. Process. https://doi.org/10.1002/HYP.11226

Soulsby, C., Malcolm, I.A., Youngson, A.F., Tetzlaff, D., Gibbins, C.N., Hannah, D.M., 2005. Groundwater-surface water interactions in upland Scottish rivers: hydrological, hydrochemical and ecological implications. Scottish J. Geol. 41, 39–49. https://doi.org/10.1144/sjg41010039

Soulsby, C., Rodgers, P., Petry, J., Hannah, D.M., Malcolm, I.A., Dunn, S.M., 2004. Using tracers to upscale flow path understanding in mesoscale mountainous catchments: Two examples from

Scotland. J. Hydrol. 291, 174–196. https://doi.org/10.1016/j.jhydrol.2003.12.042

Soulsby, C., Tetzlaff, D., van den Bedem, N., Malcolm, I.A., Bacon, P.J., Youngson, A.F., 2007. Inferring groundwater influences on surface water in montane catchments from hydrochemical surveys of springs and streamwaters. J. Hydrol. 333, 199–213. https://doi.org/10.1016/j.jhydrol.2006.08.016

Sprenger, M., Tetzlaff, D., Tunaley, C., Dick, J.J., Soulsby, C., 2017. Evaporation fractionation in a peatland drainage network affects stream water isotope composition. Water Resour. Res. 53, 851–866. https://doi.org/10.1002/2016WR019258

Taylor, R.G., Scanlon, B., Doell, P., Rodell, M., van Beek, R., Wada, Y., Longuevergne, L., Leblanc, M., Famiglietti, J.S., Edmunds, M., Konikow, L., Green, T.R., Chen, J., Taniguchi, M., Bierkens, M.F.P., MacDonald, A.M., Fan, Y., Maxwell, R.M., Yechieli, Y., Gurdak, J.J., Allen, D.M., Shamsudduha, M., Hiscock, K., Yeh, P.J.F., Holman, I., Treidel, H., 2013. Ground water and climate change. Nat. Clim. Chang. 3, 322–329. https://doi.org/10.1038/nclimate1744

Tetzlaff, D., Birkel, C., Dick, J.J., Geris, J., Soulsby, C., 2014. Storage dynamics in hydropedological units control hillslope connectivity, runoff generation, and the evolution of catchment transit time distributions. Water Resour. Res. 50, 969–985. https://doi.org/10.1002/2013WR014147

Tetzlaff, D., Carey, S.K., McNamara, J.P., Laudon, H., Soulsby, C., 2017. The essential value of long-term experimental data for hydrology and water management. Water Resour. Res. 53, 2598–2604. https://doi.org/10.1002/2017WR020838

Tetzlaff, D., Soulsby, C., 2008. Sources of baseflow in larger catchments – Using tracers to develop a holistic understanding of runoff generation. J. Hydrol. 359, 287–302. https://doi.org/10.1016/j.jhydrol.2008.07.008

Tetzlaff, D., Soulsby, C., Buttle, J., Capell, R., Carey, S.K., Laudon, H., McDonnell, J.J., Mcguire, K.J., Seibert, J., Shanley, J.B., 2013. Catchments on the cusp? Structural and functional change in northern ecohydrology. Hydrol. Process. 27, 766–774. https://doi.org/10.1002/hyp.9700

Toth, J., 1963. A Theoretical Analysis of Groundwater Flow in Small Drainage Basins 1 of phe - low order stream and having similar t he outlet of lowest impounded body of a relatively. J. Geophys. Res. 68, 4795–4812. https://doi.org/10.1029/JZ068i016p04795

Tromp-van Meerveld, H.J., McDonnell, J.J., 2006a. Threshold relations in subsurface stormflow: 1. A 147-storm analysis of the Panola hillslope. Water Resour. Res. 42, 1–11. https://doi.org/10.1029/2004WR003778

Tromp-van Meerveld, H.J., McDonnell, J.J., 2006b. Threshold relations in subsurface stormflow: 2. The fill and spill hypothesis. Water Resour. Res. 42, 1–11. https://doi.org/10.1029/2004WR003800

Wilby, R., Beven, K.J., Reynard, N.S., 2008. Climate change and fluvial flood risk in the UK: more of the same? Hydrol. Process. 2511–2523. https://doi.org/10.1002/hyp.6847

Wilby, R.L., Troni, J., Biot, Y., Tedd, L., Hewitson, B.C., Smith, D.M., Sutton, R.T., 2009. A review of climate risk information for adaptation and development planning. Int. J. Climatol. 29, 1193–1215. https://doi.org/10.1002/joc.1839

Winter, T.C., Harvey, J.W., Franke, O.L., Alley, W.M., 1998. Groundwater and Surface water a single resource. USGS Publ. Circular 1, 79.

Zimmer, M.A., McGlynn, B.L., 2017. Time-lapse animation of hillslope groundwater dynamics details event-based and seasonal bidirectional stream-groundwater gradients. Hydrol. Process. 10–12.

https://doi.org/10.1002/hyp.11124

TABLES:

Table 1: Characteristics of the deeper wells (DW) and shallower wells (ShW) showing the elevation, topographic wetness index (TWI), slope, soil type, depth of the wells, distance to the stream and distance to the outlet. Elevation, Slope and TWI were derived from a high resolution LiDAR elevation model. All wells share the same underlying bedrock type (granite) which is overlaid by glacial drift deposit.

ID	Landscape unit	Elevation [m a.s.l.]	TWI	Slope [°]	Soil type	Depth [cm]	Distance to Stream [m]	Distance to Outlet [m]	Water table relative to sea level [m a.s.l.]		
									mean	max	min
DW 1	Riparian zone	254	15.1	0.6	peat	330	7	767	254.07	254.31	253.96
DW 2	Riparian zone	254	15.5	0.6	peat	264	20	785	253.98	254.16	253.80
DW 3	Lower footslope	259	11.1	0.2	peaty gley	160	122	835	258.80	258.97	258.63
DW 4	Upper hillslope	284	2.4	18.2	peaty podzol	187	339	994	283.31	284	282.87
ShW I	Riparian zone	254	13.9	0.6	peat	90	7	769	254.05	254.26	253.87
ShW II	Lower footslope	259	9.4	1.2	peaty gley	67.2	117	841	258.73	258.84	258.59
ShW III	Upper hillslope	284	3.4	14.2	peaty podzol	63	337	985	283.75*	284.05	283.53*

* based on records, when the Odyssey logger registered a groundwater table in ShW III. ShW III could only recorded water tables > -47 cm below the surface

Table 2: Summary statistics for the groundwater wells during the 13 hysteresis events showing the pre-event discharge (Q_{pre}), the peak discharge of the event (Q_{max}), total amount of Rain during the event (P_{total}), the amount of rain seven days prior to the event (P_7), the pre-event water table in the wells (pre) and the highest recorded water table during the event (max). ShW III could only recorded water tables > -47 cm below the surface

							Riparian zone						Lower footslope				Upper hillslope			
Event	Start	End	Q_{pre}	Q_{max}	P_{total}	P_7	DW 1		DW 2		ShW I		DW 3		ShW II		DW 4		ShW III	
							pre	max	pre	max	pre	max	pre	max	pre	max	pre	max	pre	max
			[m^3/s]	[m^3/s]	[mm]	[mm]	[cm]		[cm]		[cm]		[cm]		[cm]		[cm]		[cm]	
E 1	15/08/15	17/08/15	0.04	0.19	13	8.9	0.1	7	-16	-8.7	**	**	-30.5	-22.5	-32.7	-21	-103.7	-86.6	-	-31.9
E 2	24/10/15	26/10/15	0.03	0.18	13.1	2.5	1.5	6.3	-13	-6.8	**	**	-29.5	-23.3	-31.9	-22	-93.9	-75	-	-
E 3	04/12/15	12/12/15	0.11	0.56	56.4	22.3	9.7	22.1	-1.4	7.2	8.9	26	-14.5	-8.6	-22.1	-16	-21.6	-1.2	-0.1	3.1
E 4	15/12/15	18/12/15	0.08	0.39	16.4	19.5	8.9	16.8	-0.9	1.5	8.4	25.3	-15.1	-9	-23.3	-18	-41.6	-4	-4.6	3.9
E 5	06/01/16	09/01/16	0.39	1.12	29.8	142	22.1	34.4	5.1	20.7	24.4	26	-5.2	-1.3	-20.3	-14	0.2	0.8	3.8	5.8
E 6	22/01/16	23/01/16	0.04	0.17	5.8	1.8	9.2	12.8	2.1	3.5	9.9	12.7	-14.6	-11.7	-24.6	-22	-69.3	-57.8	-44.8	-44.8*
E 7	01/02/16	03/02/16	0.08	0.45	13.4	39.4	11.5	18.8	2.3	4.9	10.4	26	-11.8	-8.5	-23.2	-14	-18.2	-1.5	2.1	3.8
E 8	22/05/16	24/05/16	0.01	0.23	16.3	13.5	6	11	0.1	4.7	-1.4	7.2	-22.9	-17.7	-27.9	-20	-102.3	-85.2	-	-46.7
E 9	14/06/16	22/06/16	0.01	0.68	70.2	15.2	3.9	23.2	-3.6	13.1	-1.4	24.7	-25.6	-6.7	-31.3	-16	-108.5	-1.4	-46.9	3.3
E 10	24/06/16	27/06/16	0.02	0.68	34.7	2	5.9	26.2	-0.3	16.5	-3.2	26	-16	-7.5	-28.4	-16	-71.8	-4.3	-34.7	1
E 11	11/07/16	11/07/16	0.03	0.41	9.9	23.3	8.7	17.8	5.7	8.9	4.6	15.8	-15.7	-12.6	-23.8	-18	-86.7	-63.7	-	-39.5
E 12	24/07/16	24/07/16	0.005	0.11	11.7	27.2	8.5	13.7	5.2	8.4	3.1	9.9	-16.5	-12.4	-25.9	-20	-69.5	-51.3	-	-45.4
E 13	02/08/16	02/08/16	0.005	0.09	10.5	6.5	6.4	11.1	3.4	7.3	2.2	9.4	-18.9	-14.2	-26.9	-20	-90.4	-75.1	-	-

* ShW III showed no response during that event, water level was declining inside the well

** ShW II was not yet deployed during these events

Table 3: Hysteresis Index (HI_{LL}) values for the groundwater wells during the 13 different events (E1-13); negative values indicate anticlockwise and positive values clockwise behaviour; the values can range from -1 to 1 and large values indicate the "fatness" of simple loops; Dir = hysteresis direction, A = anti-clockwise, C = clockwise, ^{8} = indicating a figure-of-eight shape and ** = indicating a more complex shape; Lag time between the peaks in hours for the events, mean and the weighted mean based on occurrence of – or + values, positive values in lag time indicate that the stream to peaks before and the well and negative values indicate vice versa.

* ShW III recorded a rather steady groundwater table during E6 only ranging from -46.9 to -46.7, it was not possible to calculate the HI_{LL}

Event	Riparian zone									Lower footslope						Upper hillslope					
	DW 1			DW 2			ShW I			DW 3			ShW II			DW 4			ShW III		
	HI_{LL} [-]	Dir	Lag time [h]	HI_{LL} [-]	Dir	Lag time [h]	HI_{LL} [-]	Dir	Lag time [h]	HI_{LL} [-]	Dir	Lag time [h]	HI_{LL} [-]	Dir	Lag time [h]	HI_{LL} [-]	Dir	Lag time [h]	HI_{LL} [-]	Dir	Lag time [h]
E 1	-0.37	A	-0.5	-0.51	A	20	-	-	-	-0.56	A	20.5	-0.2	A^{8}	-1.75	-0.39	A	34	-0.52	A	1
E 2	-0.47	A	6.5	-0.42	A	15.3	-	-	-	-0.58	A	18.5	-0.23	A	0.25	-0.51	A	42.5	-	-	-
E 3	-0.13	A^{**}	-0.75	-0.17	A^{**}	0	0.02	C^{**}	-3.5	-0.45	A^{**}	18.5	0.26	C^{**}	-2.25	-0.46	A^{**}	18	-0.35	A^{**}	113
E 4	-0.21	A^{8}	-1.5	-0.09	A^{8}	-1.5	0.04	C^{8}	-1.25	-0.49	A	15.25	0.17	C	-0.25	-0.69	A	32.5	-0.43	A	32.75
E 5	0.01	C^{8}	1.5	0	C^{8}	1.25	-0.07	$A^{\sim}$	-14	-0.22	A	7.25	0.36	C	-4	-0.08	A^{**}	29.3	0.12	C^{**}	0.75
E 6	-0.39	A	3.5	-0.31	A^{**}	4	-0.07	A^{8}	1	-0.64	A	7.25	0.39	C	-2.5	-0.53	A	34.3	***	-	***
E 7	-0.1	A	-0.25	-0.38	A	0.25	-0.01	A^{8}	-1.25	-0.7	A	16	0.42	C	-3.75	-0.48	A	14.3	0.35	C	-3.5
E 8	-0.33	A	0.25	-0.09	A	26	-0.03	A^{8}	-0.75	-0.34	A	15	0.23	C	-2	-0.33	A	43.5	*	-	-
E 9	-0.26	A^{**}	13	-0.22	A^{**}	-0.5	0.04	C^{8}	-0.25	-0.53	A^{**}	41.25	0.16	C^{**}	-2	-0.69	A^{**}	58.3	-0.23	A^{**}	48.5
E 10	-0.07	A^{**}	0	-0.09	A^{**}	1	0.13	C^{**}	-1	-0.32	A^{**}	19.75	0.16	C^{**}	-1.75	-0.39	A^{**}	27.3	-0.26	A^{**}	30.75
E 11	-0.25	A	0	-0.24	A	0.75	0.18	C^{8}	-1	-0.37	A	5.75	0.36	C	-3.25	-0.56	A	20.8	-0.3	A	3
E 12	-0.22	A	-0.25	-0.2	A	16.3	0.09	C^{8}	-0.25	-0.28	A	15.75	0.23	C	-2.75	-0.53	A	15.8	-0.66	A	5.25
E 13	-0.33	A	-0.25	-0.22	A	12.8	0.1	C^{8}	-0.5	-0.36	A	9.75	0.26	C	-2.25	-0.39	A	14.3	-	-	-
Mean	-0.24	A	1.63	-0.23	A	7.35	0.04	C^{8}	-2.07	-0.45	A	16.19	0.20	C	-2.17	-0.46	A	29.58	-0.25	A	25.72
Weighted mean	-0.24	-	1.63	-0.23	-	7.35	0.04	-	-2.07	-0.45	-	16.19	0.21	-	-2.17	-0.46	-	29.58	-0.25	-	25.72

*** ShW III did not response to the during Event 4, the water level was consistently declining

~ likely to directly affected by flooding of the riparian area

Table 4: a) Correlation coefficients and lag times between the time series of the stream and the different monitored groundwater tables along the hillslope. These values considered the whole time series and only reflect the overall behaviour between the time series. Positive values in time shift indicate that the stream tends to peak before and the well and negative values indicate vice versa; * $P < 0.05$.

b) Lag times for the main discharge peak on the December 30th, 2015 during the winter flood compared to the mean lag times during the events.

Table 4a)

Time series	Landscape	correlation coefficient [-]	Lag time [h]
Stream/DW 1	Riparian zone	0.70*	0.75
Stream/DW 2	Riparian zone	0.36*	0.75
Stream/DW 3	Lower footslope	0.51*	9
Stream/DW 4	Upper hillslope	0.57*	10.5
Stream/ShW I	Riparian zone	0.85*	-0.25
Stream/ShW II	Lower footslope	0.46*	-2.25
Stream/ShW III+	Upper hillslope	0.58*	10.5

Table 4b)

Time series	Landscape	Flood peak lag time [h]	Mean event lag time [h]
Stream/DW 1	Riparian zone	1.25	1.63
Stream/DW 2	Riparian zone	1.50	7.35
Stream/DW 3	Lower footslope	5.00	16.19
Stream/DW 4	Upper hillslope	Inconclusive, due persistently high GW table very close to the surface	29.58
Stream/ShW I	Riparian zone	Inconclusive, high GW table exceed the measuring capabilities of the logger. Logger was likely submerged under water during that time.	-2.07
Stream/ShW II	Lower footslope	1.5	-2.17
Stream/ShW III+	Upper hillslope	-1.75	25.72

+ only the monitored values were considered

Table 5: Summary statistics of the vol. soil moisture content (vsmc) during 13 hysteresis events showing the pre-event discharge (Q_{pre}), the peak discharge of the event (Q_{max}), total amount of Rain during the event (P_{total}), the amount of rain seven days prior to the event (P_7), the pre-event vsmc at the different soil depths (pre) and the highest recorded vsmc during the event (max).

							Riparian zone / Peat		Lower footslope / Peaty gley						Upper hillslope / Peaty podzol					
Event	Start	End	Q_{pre}	Q_{max}	P_7	P_{total}	10 cm		10 cm		30 cm		50 cm		10 cm		30 cm		50 cm	
			[m^3/s]	[m^3/s]	[mm]	[mm]	pre [v/v]	max [v/v]	pre [v/v]	max [v/v]	pre [v/v]	max [v/v]	pre [v/v]	max [v/v]	pre [v/v]	max [v/v]	pre [v/v]	max [v/v]	pre [v/v]	max [v/v]
E 1	15/08/2015	17/08/2015	0.04	0.19	8.9	13	0.82	0.82	0.69	0.71	0.39	0.39	0.36	0.36	0.3	0.33	0.26	0.27	0.28	0.3
E 2	24/10/2015	26/10/2015	0.03	0.18	2.5	13.1	0.83	0.83	0.72	0.73	0.4	0.4	0.36	0.36	0.31	0.34	0.27	0.28	0.29	0.31
E 3	04/12/2015	12/12/2015	0.11	0.56	22.3	56.4	0.84	0.84	-	-	-	-	-	-	0.36	0.44	0.34	0.38	0.36	0.39
E 4	15/12/2015	18/12/2015	0.08	0.39	19.5	16.4	0.84	0.84	0.74	0.74	0.4	0.4	0.36	0.36	0.36	0.41	0.31	0.38	0.34	0.37
E 5	06/01/2016	09/01/2016	0.39	1.12	142	29.8	0.84	0.84	0.74	0.75	0.4	0.4	0.36	0.36	-	-	-	-	-	-
E 6	22/01/2016	24/01/2016	0.04	0.17	1.8	5.8	0.85	0.85	0.75	0.75	0.4	0.4	0.36	0.36	0.35	0.36	0.29	0.3	0.32	0.33
E 7	01/02/2016	03/02/2016	0.08	0.45	39.4	13.4	0.84	0.84	0.75	0.75	0.4	0.4	0.36	0.36	0.37	0.41	0.34	0.38	0.36	0.38
E 8	22/05/2016	24/05/2016	0.01	0.23	13.5	16.3	0.83	0.83	0.72	0.74	0.4	0.4	0.36	0.36	0.31	0.33	0.26	0.27	0.28	0.3
E 9	14/06/2016	22/06/2016	0.01	0.68	15.2	70.2	0.81	0.82	0.71	0.74	0.39	0.39	0.36	0.36	0.29	0.45	0.25	0.39	0.27	0.39
E 10	24/06/2016	27/06/2016	0.02	0.68	2	34.7	0.81	0.81	0.72	0.74	0.39	0.39	0.36	0.36	0.33	0.42	0.29	0.37	0.31	0.38
E 11	11/07/2016	12/07/2016	0.03	0.41	23.3	9.9	0.81	0.81	0.73	0.73	0.39	0.39	0.36	0.36	0.32	0.36	0.27	0.28	0.3	0.32
E 12	24/07/2016	25/07/2016	0.005	0.11	27.2	11.7	0.8	0.8	0.72	0.73	0.39	0.39	0.36	0.36	0.33	0.36	0.28	0.29	0.31	0.32
E 13	02/08/2016	03/08/2016	0.005	0.09	6.5	10.5	0.8	0.8	0.72	0.73	0.39	0.39	0.36	0.36	0.31	0.34	0.27	0.28	0.3	0.31

Table 6: Hysteresis Index (HI_{LL}) values of the vol. soil moisture content during the 13 different events (E1-13); negative values indicate anticlockwise and positive values clockwise behaviour; the values can range from -1 to 1 and large values indicate the "fatness" of simple loops; Dir = hysteresis direction, A = anti-clockwise, C = clockwise, [8] = indicating a figure-of-eight shape and [**] = indicating a more complex shape; Lag time between the peaks in hours for the events and the mean, positive values in lag time indicate that the stream to peaks before and the soil and negative values indicate vice versa. On the lower footslope, no changes in in vol. soil moisture content was recorded during the events at the depths of 30 and 50 cm. Hence, they are not part of this table.

Event	Riparian zone / Peat			Lower footslope / Peaty gley*			Upper hillslope / Peaty podzol								
	10 cm			10 cm			10 cm			30 cm			50 cm		
	HI_{LL} [-]	Dir	Lag time [h]	HI_{LL} [-]	Dir	Lag time [h]	HI_{LL} [-]	Dir	Lag time [h]	HI_{LL} [-]	Dir	Lag time [h]	HI_{LL} [-]	Dir	Lag time [h]
E 1	*	-	*	-0.17	A**	-4.5	0.06	C[8]	-4	-0.97 [RP,S]	A	-2.25	-0.73 [RP,S]	A	0.75
E 2	*	-	*	0.93[S]	C	-5	0.15	C[8]	-3	-1 [RP]	A	-0.25	0.16	C**	-3
E 3	*	-	*	-	-	-	-0.2	A**	-2.75	-0.36	A**	-3.25	-0.38	A**	-3
E 4	*	-	*	*	-	*	-0.6	A	4.25	-0.79	A	2.5	-0.56	A	1
E 5	*	-	*	1[S]	C	-5	-	-	-	-	-	-	-	-	-
E 6	*	-	*	*	-	*	-0.9 [RP,S]	A	-2.25	-0.97 [RP,S]	A	6.5	-1 [RP,S]	A	-4
E 7	*	-	*	*	-	*	0.18	C**	-3.5	-0.11	A**	-1.75	0.41	C**	-4
E 8	*	-	*	-0.5	A**	4.8	-0.2	C[8]	-2.75	-0.99[S]	A	1	-0.44	A[8]	-2.8
E 9	-1[S]	A	19.5	-0.33	A**	-5.5	-0.2	A**	-2	-0.5	A[8]	-2	-0.38	A[8]	-2.8
E 10	*	-	*	-0.49 [RP]	A**	9.5	-0.3	A**	-2	-0.3	A**	-1.25	-0.26	A**	-1.8
E 11	*	-	*	*	-	*	0.26	C	-4.25	-0.95[S]	A	-1.75	0.37 [RP]	C	-4.3
E 12	*	-	*	-0.97 [RP,S]	A	0.8	0.21	A[8]	-3.75	-0.77 [RP,S]	A	-2.75	-1 [RP,S]	A[8]	-3.8
E 13	*	-	*	-0.93 [S]	A	3.5	0.36	C	-4.25	-0.62 [RP,S]	A	6	0.85 [RP,S]	C	-4.3
Mean	-1	-	19.50	-0.18		-0.19	-0.10		-2.52	-0.69	A	0.06	-0.40	A	-2.22

*no changes in vol. soil moisture content during the event at the depths of 30 and 50 cm

[RP] vsmc rose during the event and didn't change for the remainder of the event

[S] high Hysteresis index, due to small actual changes in vsmc

Figure 1: Bruntland Burn catchment showing a) an aerial photograph of the study site and location of the deeper wells (DW), shallower wells (ShW) and soil moisture stations near DW 2, 3 and 4, weather station and stream gauge; b) predominant bedrock types and the extent of the overlying drift deposit; c) the predominant soil types.

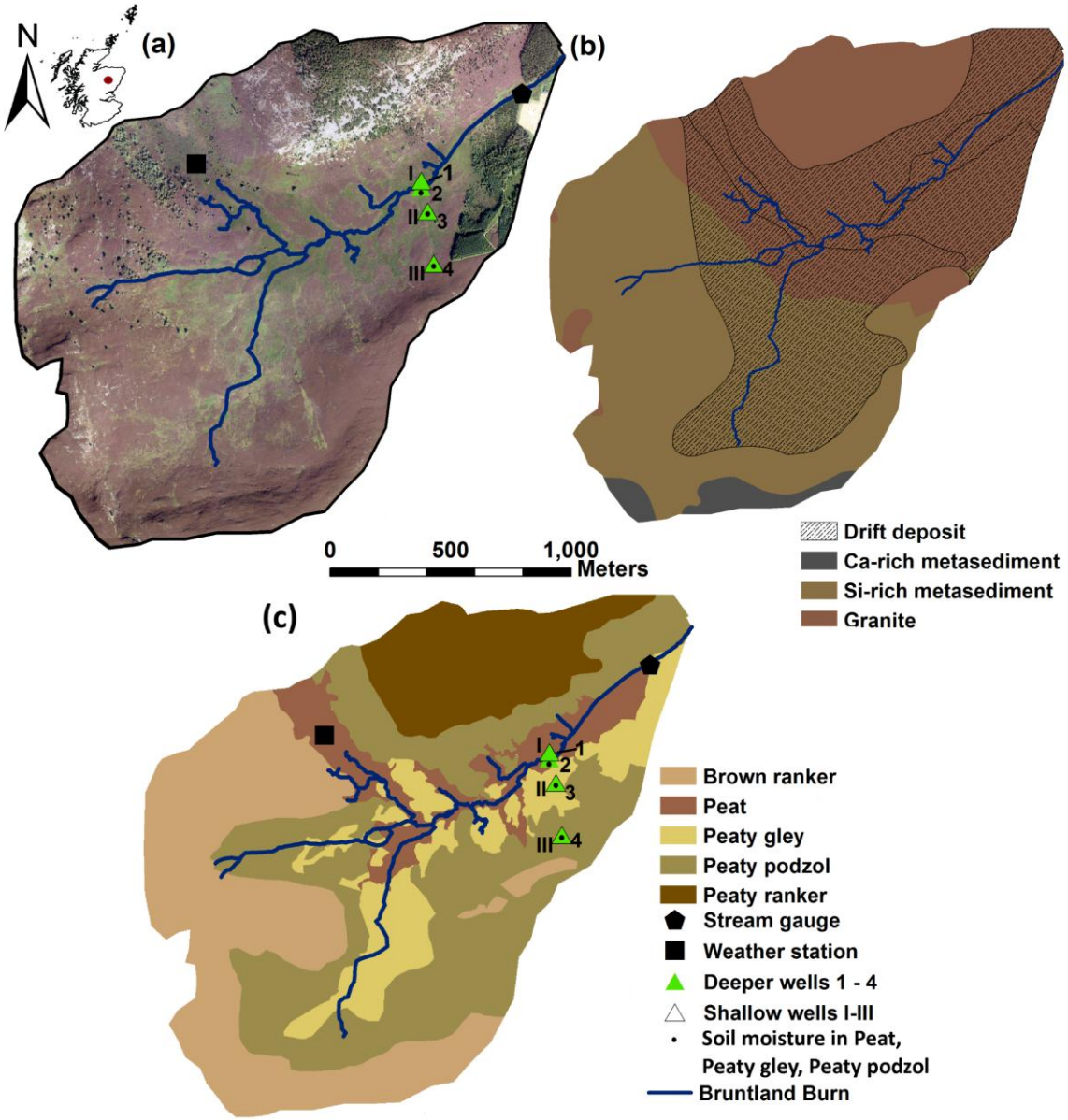
N
(a)
(b)
(c)
I
1
2
II
3
III
4
0
500
1,000
Meters
Drift deposit
Ca-rich metasediment
Si-rich metasediment
Granite
Brown ranker
Peat
Peaty gley
Peaty podzol
Peaty ranker
Stream gauge
Weather station
Deeper wells 1 - 4
Shallow wells I-III
Soil moisture in Peat, Peaty gley, Peaty podzol
Bruntland Burn

Figure 2: Schematic profile (not to scale) of the north-facing hillslope showing the depths of the monitored wells

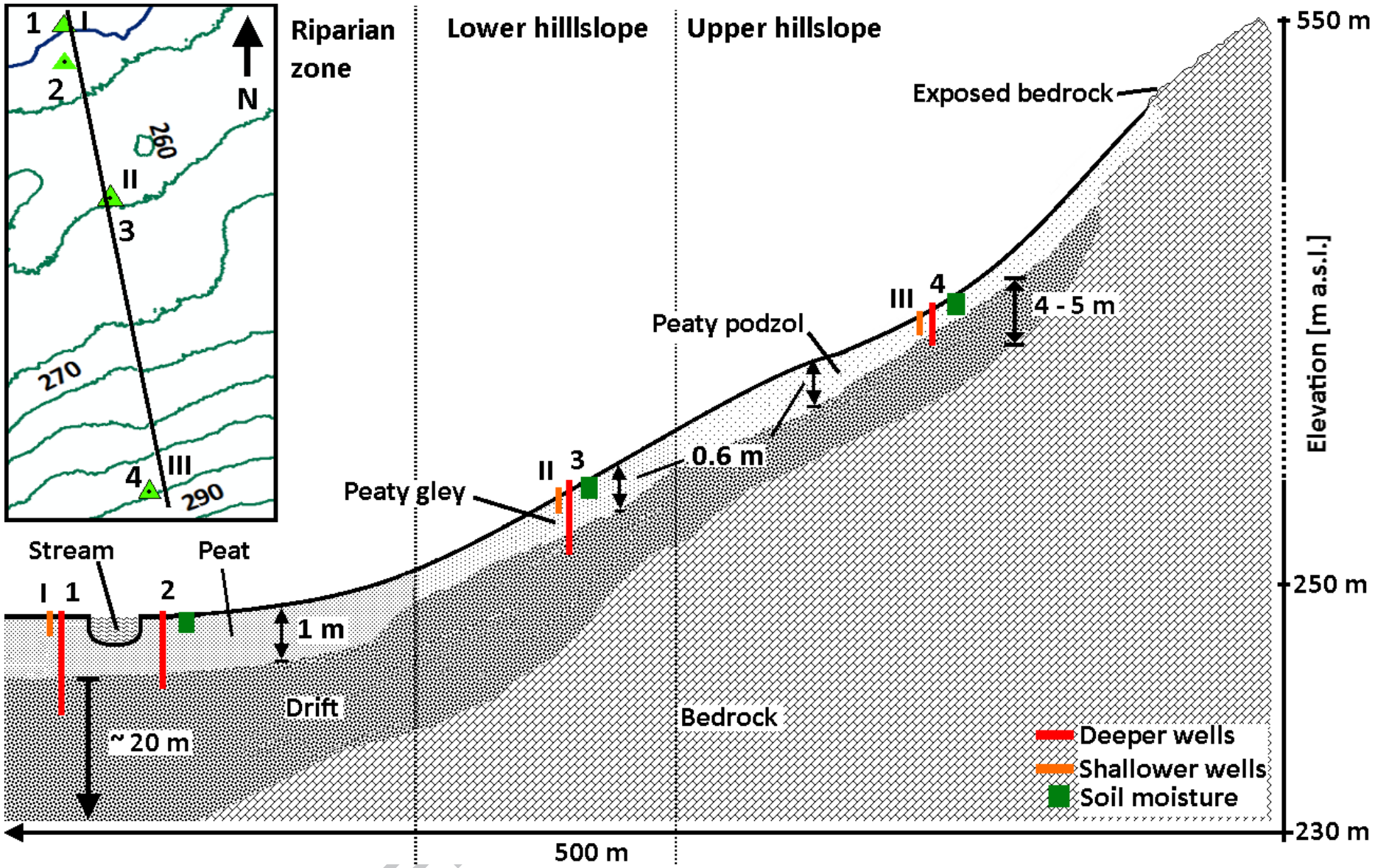
1
I
2
N
260
II
3
270
4
III
290
Riparian zone
Lower hilllslope
Upper hillslope
550 m
Exposed bedrock
Peaty podzol
III
4
4 - 5 m
Elevation [m a.s.l.]
Peaty gley
II
3
0.6 m
Stream
Peat
I
1
2
1 m
Drift
~ 20 m
Bedrock
250 m
Deeper wells
Shallower wells
Soil moisture
230 m
500 m

Figure 3: Time series of daily (a) precipitation and discharge at the outlet; (b) groundwater levels of the 4 deeper wells (DW 1 - 4); (c) groundwater levels of the 3 shallower wells (ShW I - III), the red line represents the approximated values for ShW III; (d) water temperature inside the deeper wells; the grey areas in a) - c) indicate the events (E1 - 13) chosen for the hysteresis analysis. As ShW III was mostly dry during the study period (~207 Days) and only active during larger storm events, we estimated the behaviour of the well below this threshold for figure 3c, but only used recorded values for the statistical analysis.

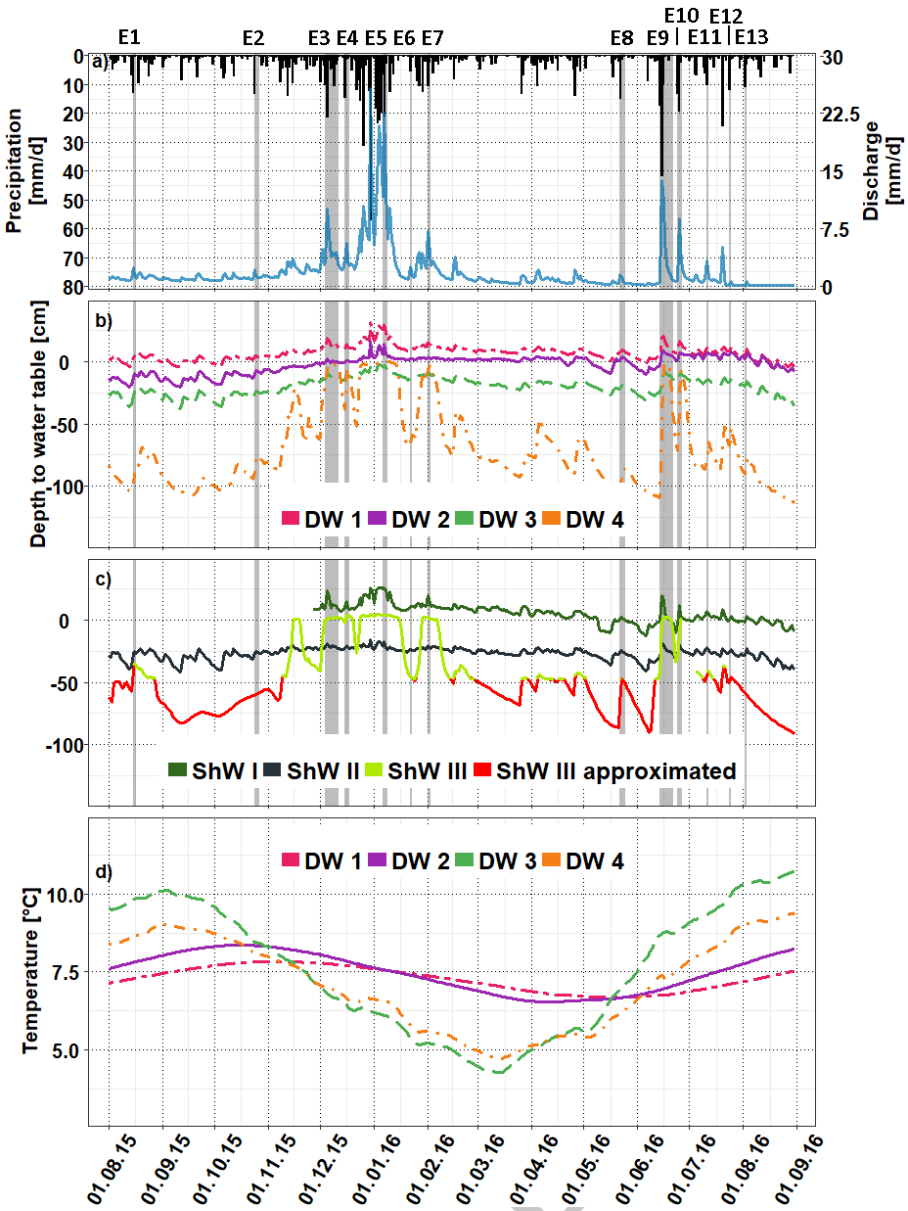

Figure 4: a) the hourly precipitation [mm h^{-1}] and Discharge [m^3 s^{-1}] in 15 min interval, b) the hourly mean groundwater level in the deeper wells (DW 1 - 4), c) the daily mean volumetric soil moisture content in the c.1) riparian zone, c.2) lower footslope and the c.3) upper hillslope and d) the day-to-day δ^2H of precipitation (black stars) and the stream water (blue dots) for the period between 22/12/2015 - 18/01/2016. The data gap was caused equipment failure during the extreme precipitation events.

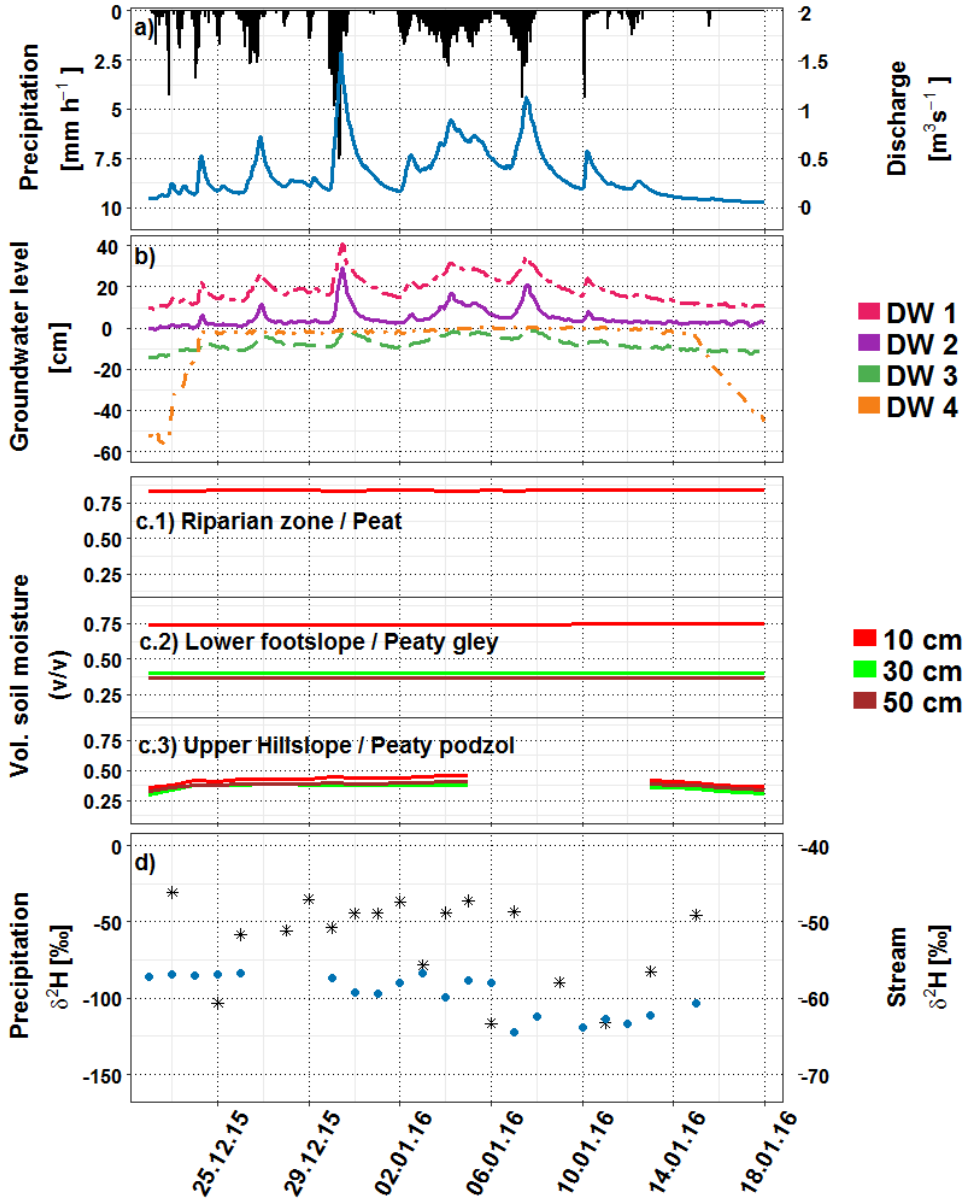

Figure 5: Time series of daily (a) precipitation and discharge at the outlet; (b) volumetric soil moisture content in the first 10 cm of the organic layer in riparian zone (peat soil); (c) volumetric soil moisture content in the first 10 cm in the organic layer and the two mineral layers at 30 cm and 50 cm depth on the lower footslope in the transitional zone (peaty gley soil); (d) volumetric soil moisture content in the first 10 cm in the organic layer and the two mineral layers at 30 cm and 50 cm depth on the upper footslope (peaty podzol soil); the grey areas in a) - d) indicate the events (E1 – 13) chosen for the hysteresis analysis.

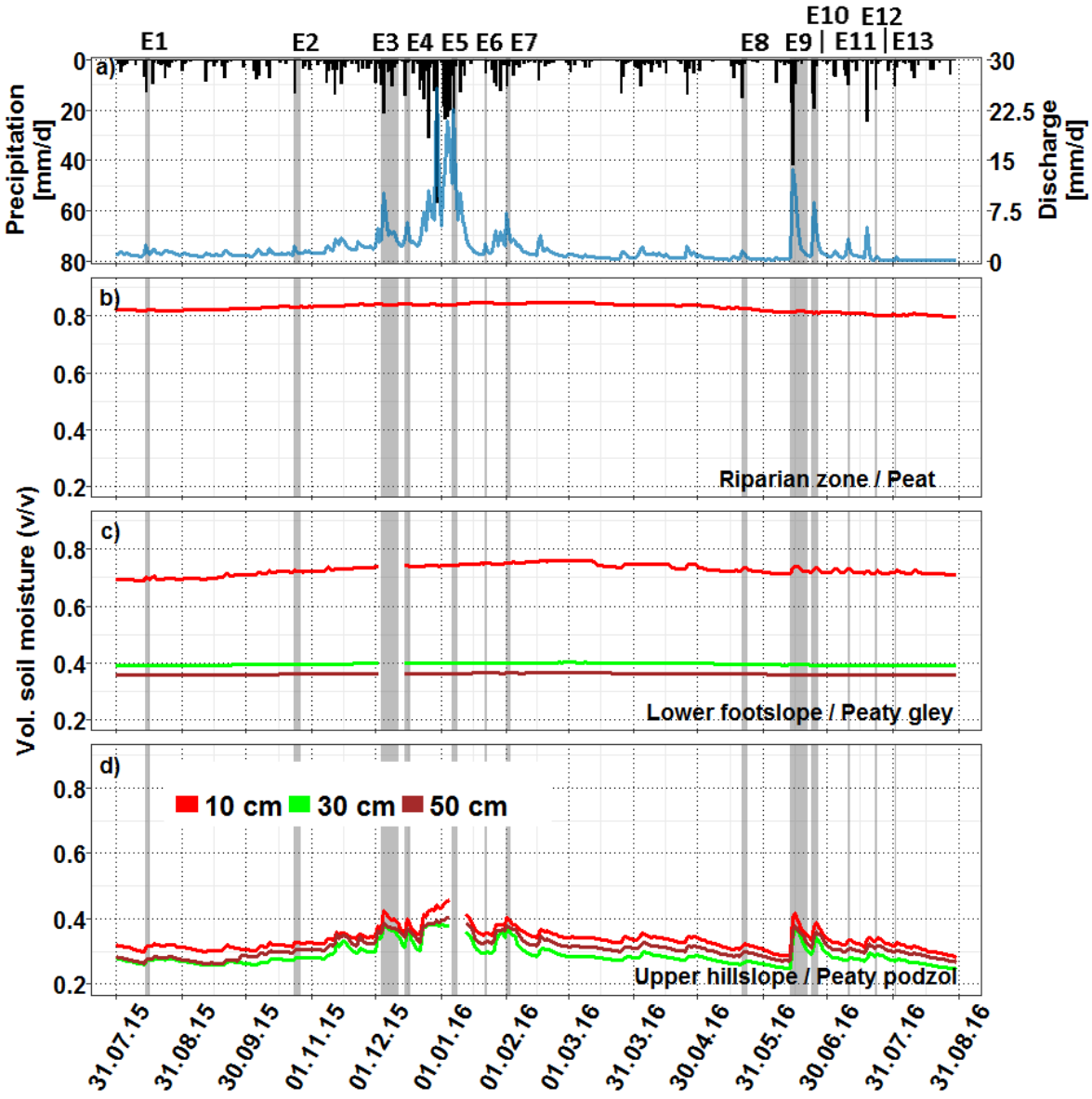

Figure 6: Event 3 (E 3); hysteresis plots of normalized stream discharge vs depth to water tables during an event between the 15.12. – 18.12.2015;

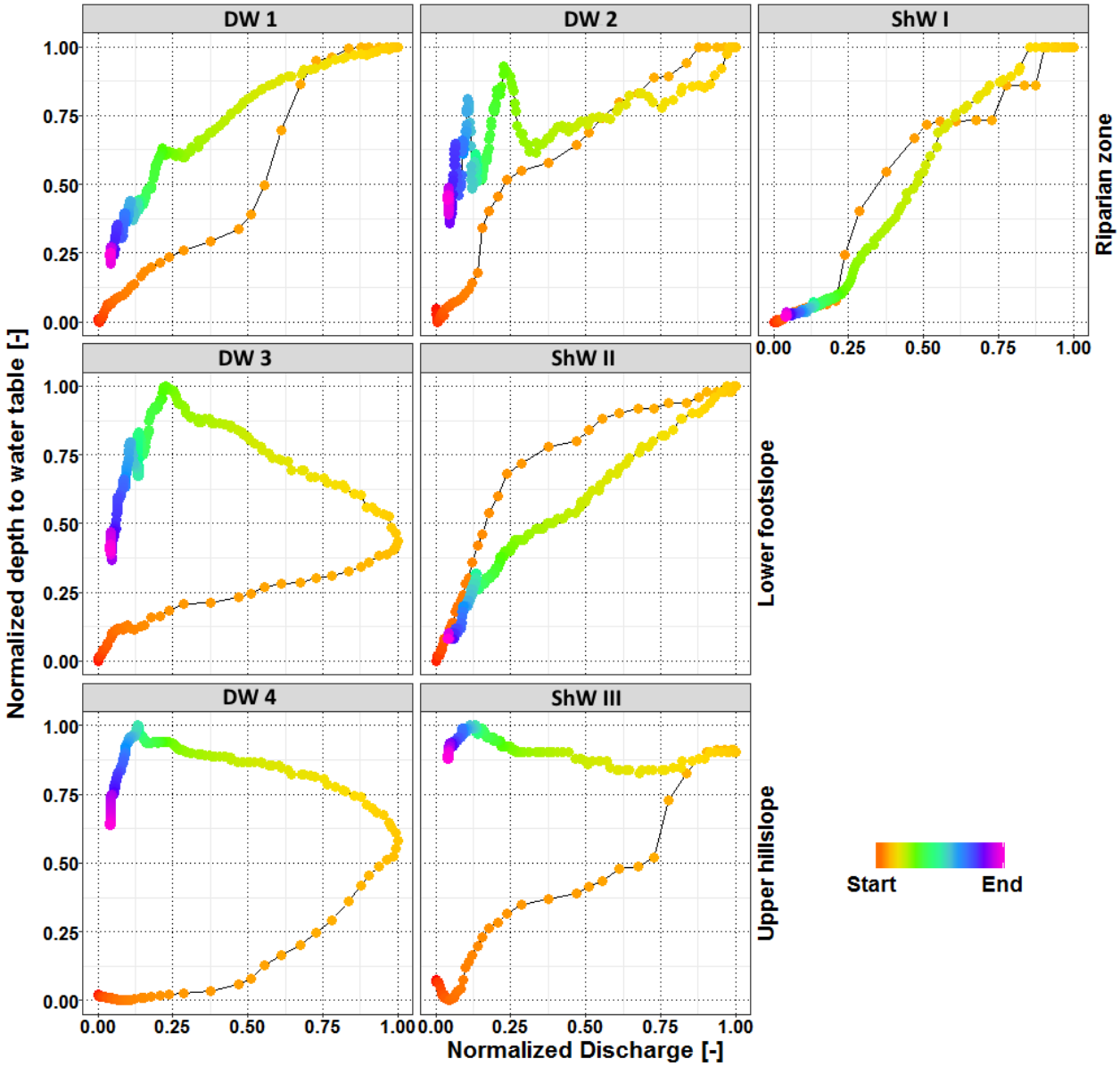

Figure 7: Event 7 (E7); hysteresis plots of normalized stream discharge vs depth to water tables during an event between the 14th June 2016 and 22nd June 2016; this event had to large discharge peaks in short succession.

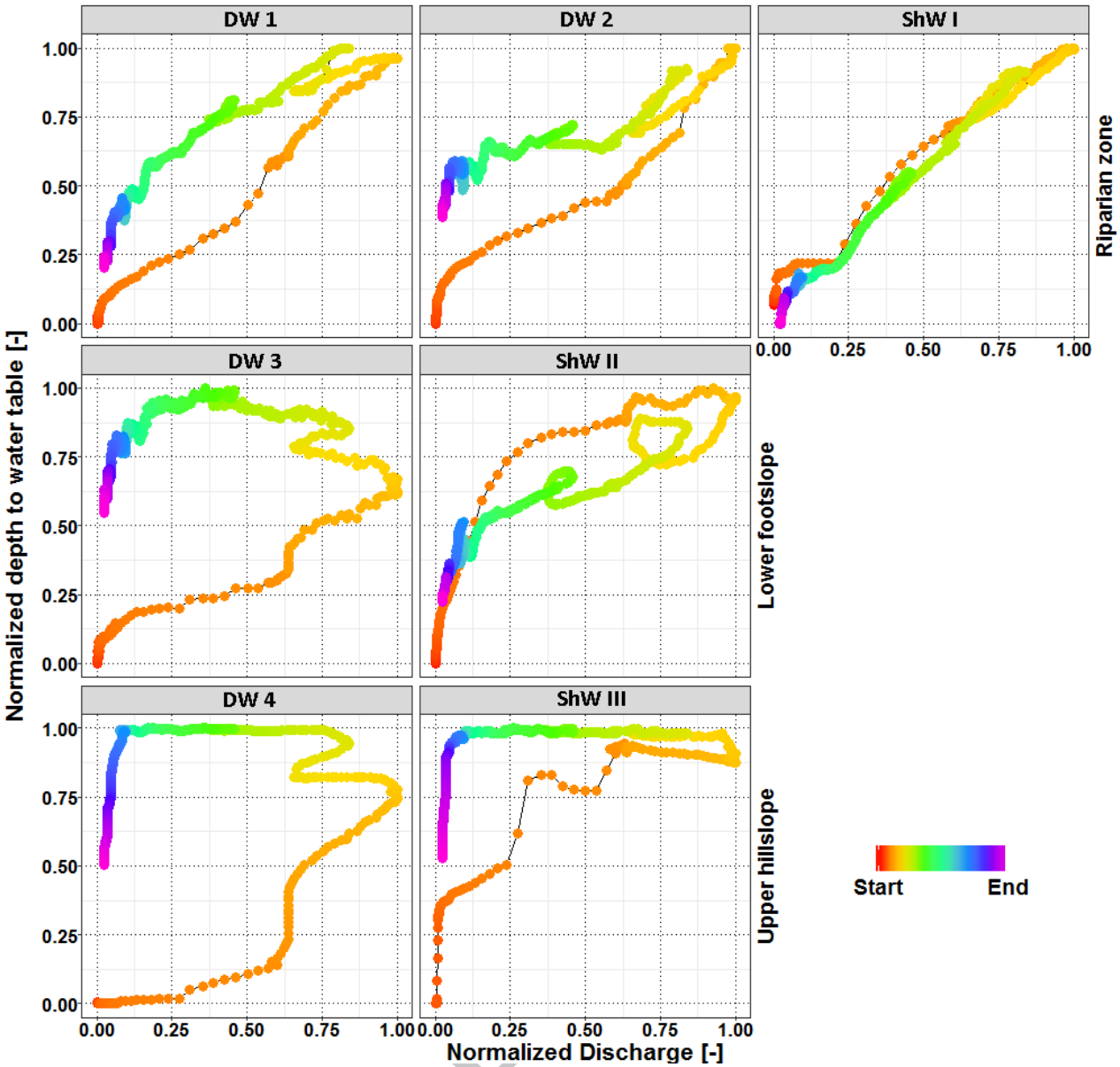
DW 1
DW 2
ShW I
DW 3
ShW II
DW 4
ShW III
Riparian zone
Lower footslope
Upper hillslope
Normalized depth to water table [-]
Normalized Discharge [-]
0.00
0.25
0.50
0.75
1.00
Start
End

Figure 8: Hysteresis plots of normalized discharge vs the normalized groundwater tables during the extreme event between the 22th December 2015 and 18th January 2016

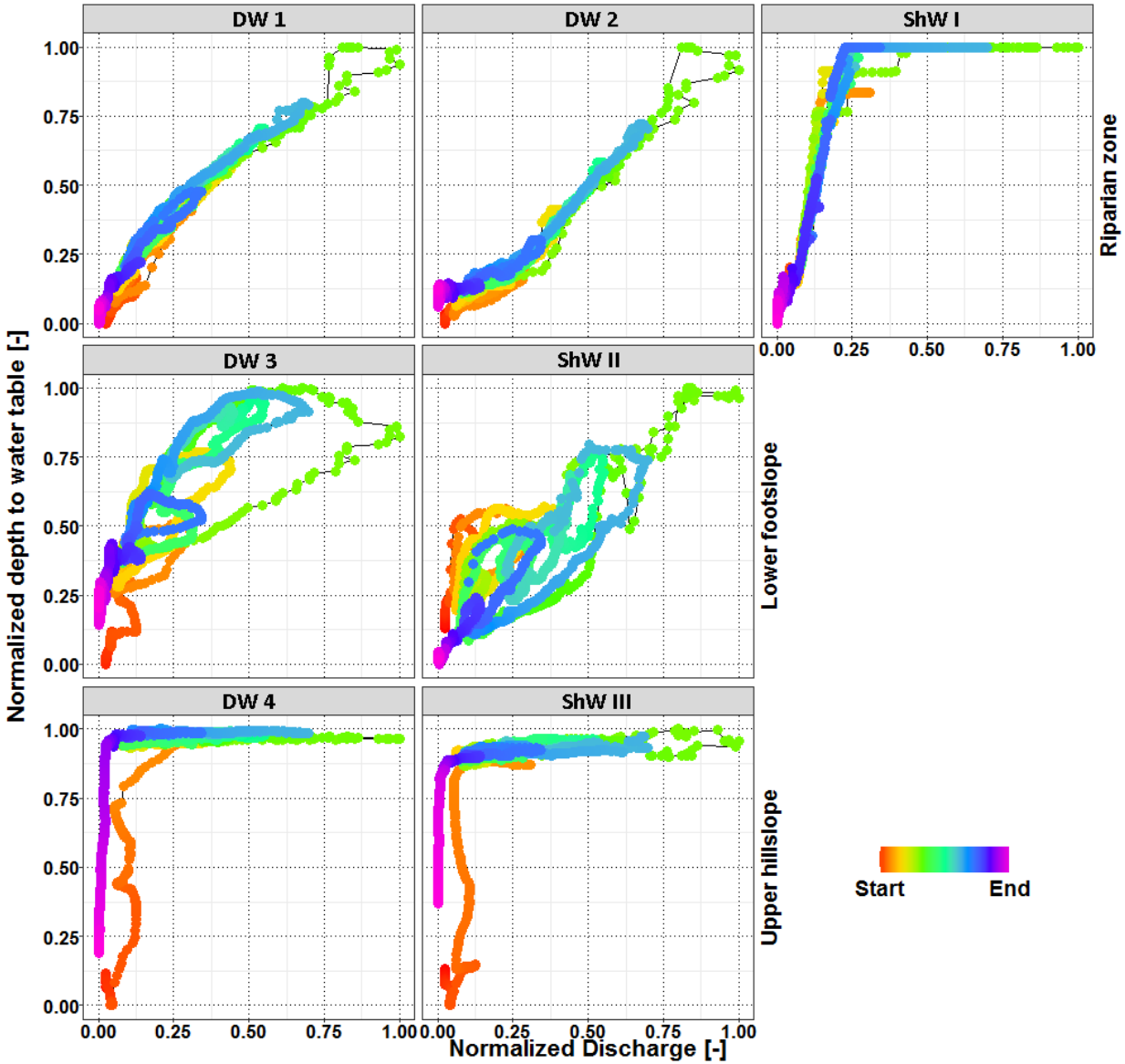

Figure 9: Isotope signature of the groundwater wells in respect to the signature of the stream at the outlet and the precipitation.

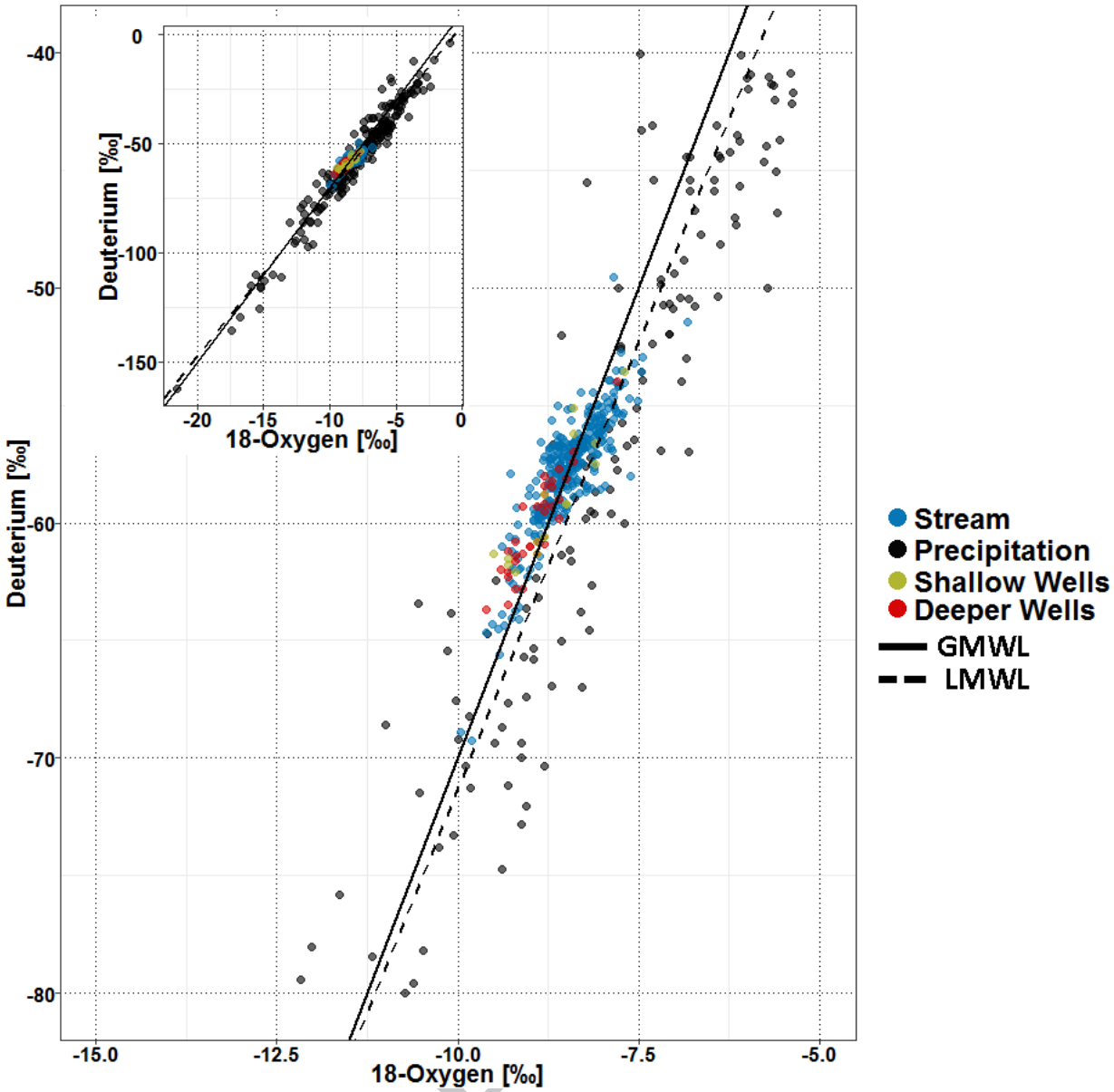

Figure 10: Boxplots for a) deuterium and b) lc-excess of the 4 deeper (DW 1 – DW 4) and 3 shallower wells (ShW I - III) with the colour code reflecting the depth of the wells; the capital letters indicate the corresponding landscape unit (RZ – Riparian zone, LF – Lower footslope, UH – Upper hillslope)

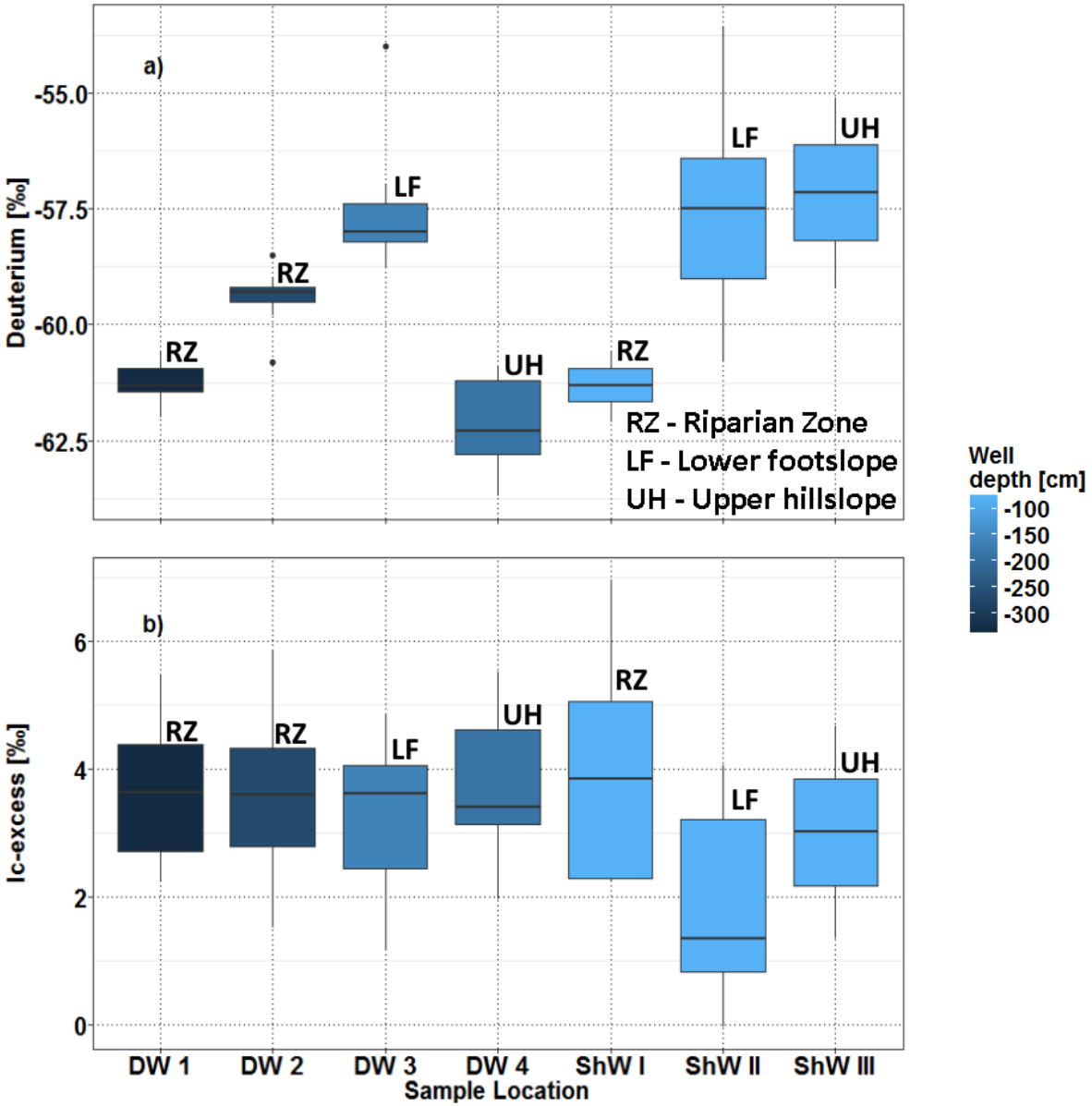

Figure 11: Time series of (a) daily precipitation (black) and discharge at the outlet (blue), (b) deuterium and the (c) lc-excess signal.

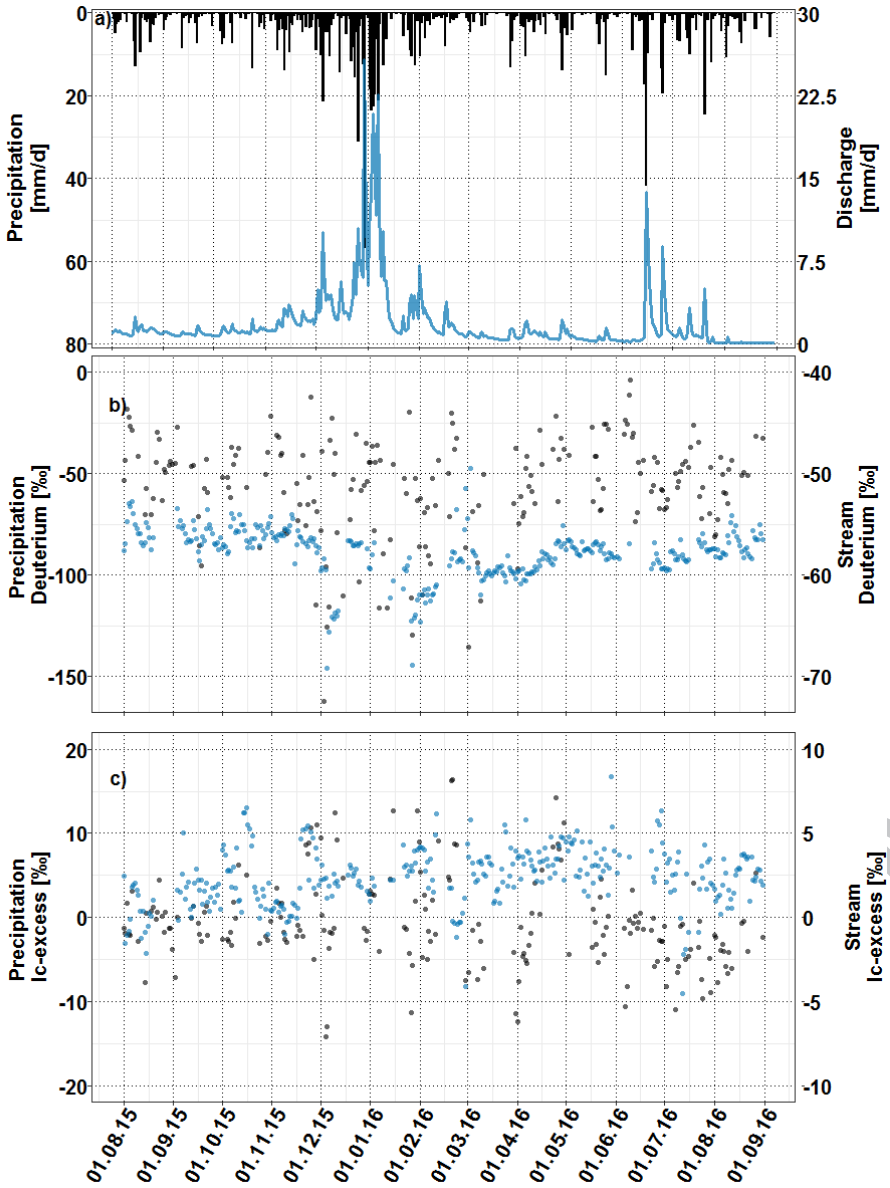

Figure 12: Conceptual cross-section of catchment emphasizing on the groundwater isotope signal. The widths of the arrows indicates depletion of the groundwater signal, the wider the arrow the more depleted the isotope signal. The lengths indicates the mixing, short arrows little mixing and long arrows vice versa. The groundwater on the upper hillslope and in the riparian zone was more depleted than on the lower footslope, but on the upper hillslope the groundwater was less affected by mixing processes compared to the rest of the transect

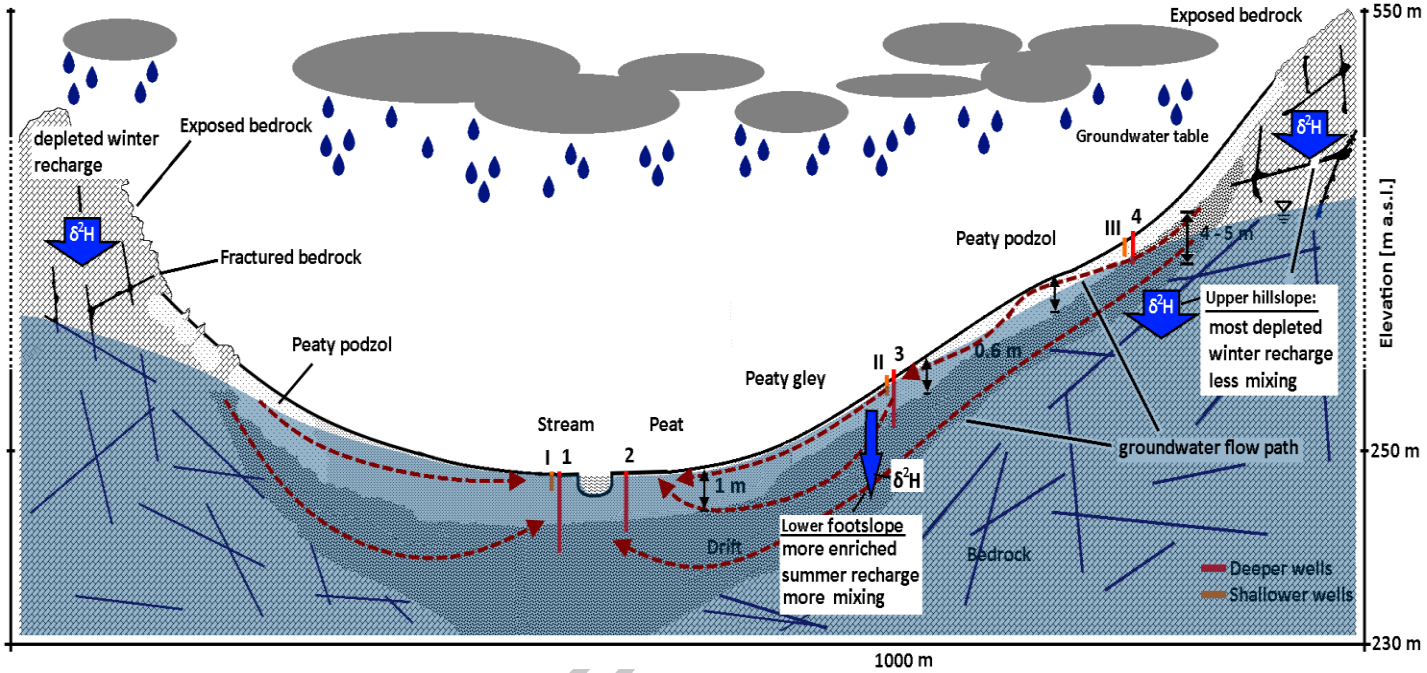

Highlights

We monitored GW-SW dynamics along a hillslope transect during a >200 year flood

Artesian GW behaviour in riparian zone and on upper hillslope

Deeper GW response slower than fast responding shallower GW during events

Isotopes reveal remarkably well-mixed GW system recharged by winter precipitation